

Electronic Supplementary Information

1,10-Phenanthroline-dithiine iridium and ruthenium complexes: Synthesis, characterization and photocatalytic dihydrogen evolution

Elisa Erdmann,^{a,b} Alexander Villinger,^a Burkhard König,^{*b} and Wolfram W. Seidel^{*a}

^a Institut für Chemie, Universität Rostock, Albert-Einstein-Straße 3a, 18059 Rostock, Germany

^b Institut für Organische Chemie, Fakultät für Chemie und Pharmazie, Universität Regensburg, Universitätsstraße 31, 93053 Regensburg

I	Additional NMR spectroscopic data	S2
II	Additional information on structure, photoluminescence and absorption measurements	S16
III	Additional information on photocatalysis	S26

I Additional NMR spectroscopic data

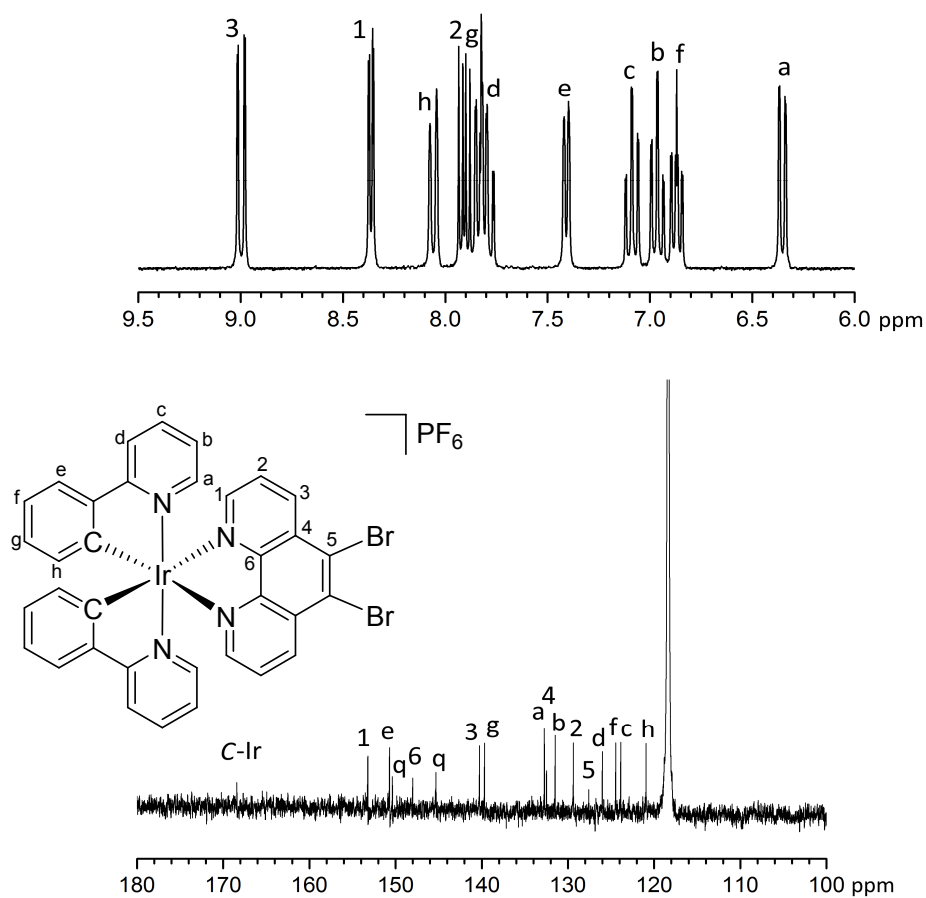


Figure S1. Top: ¹H NMR spectrum of **2-PF₆** in CD₃CN at 300 K; bottom: ¹³C NMR spectrum of **2-PF₆** in CD₃CN at 300 K.

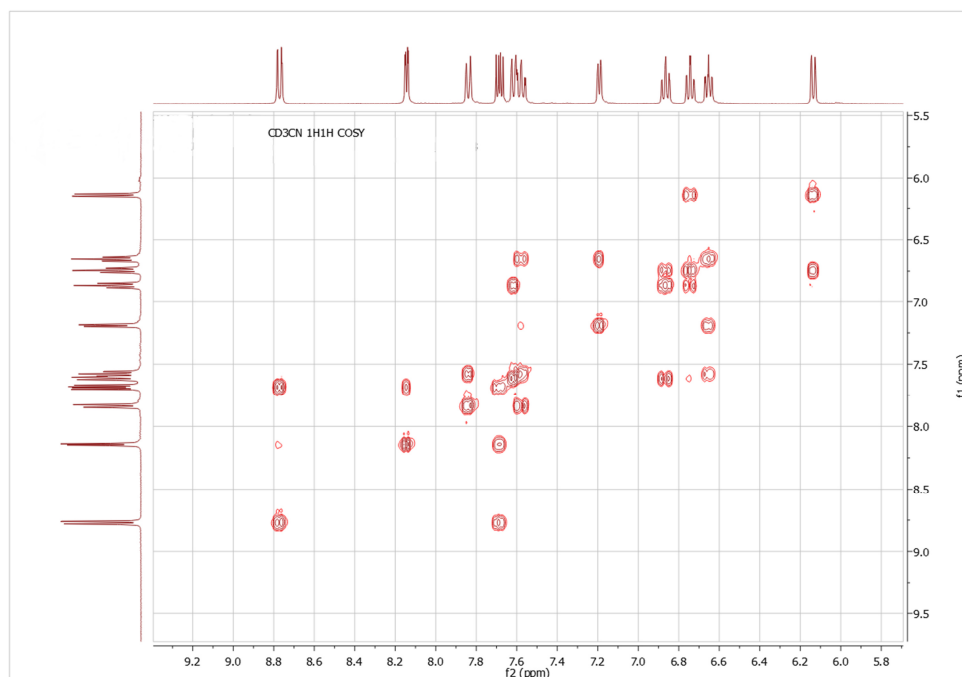


Figure S2. ¹H-¹H COSY NMR spectrum of **2-PF₆** in CD₃CN at 300 K.

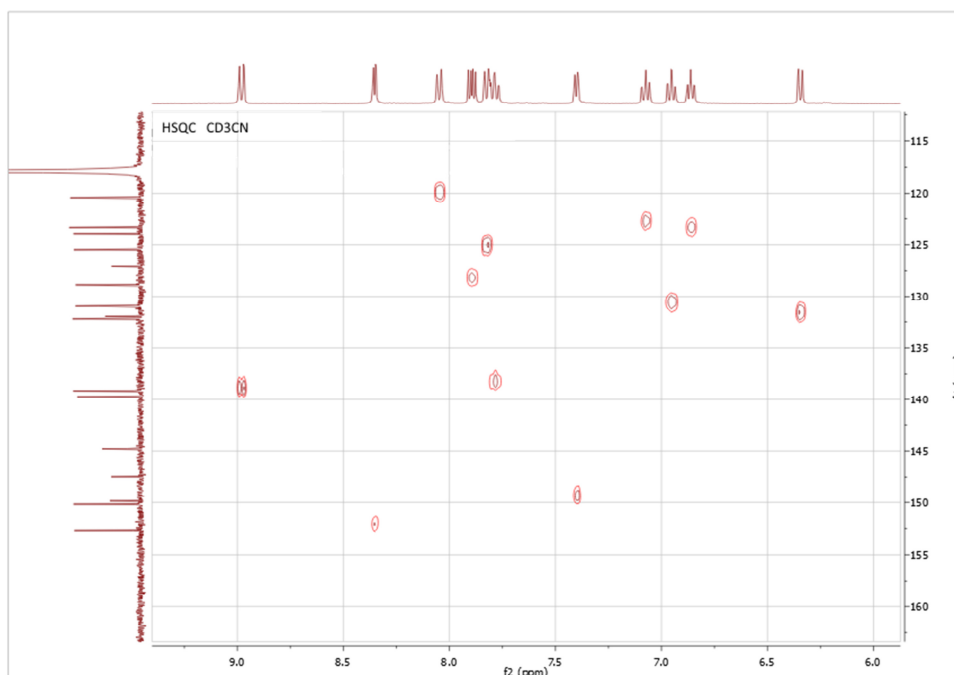


Figure S3. $^1\text{H}^{13}\text{C}$ HSQC NMR spectrum of **2**-PF₆ in CD₃CN at 300 K.

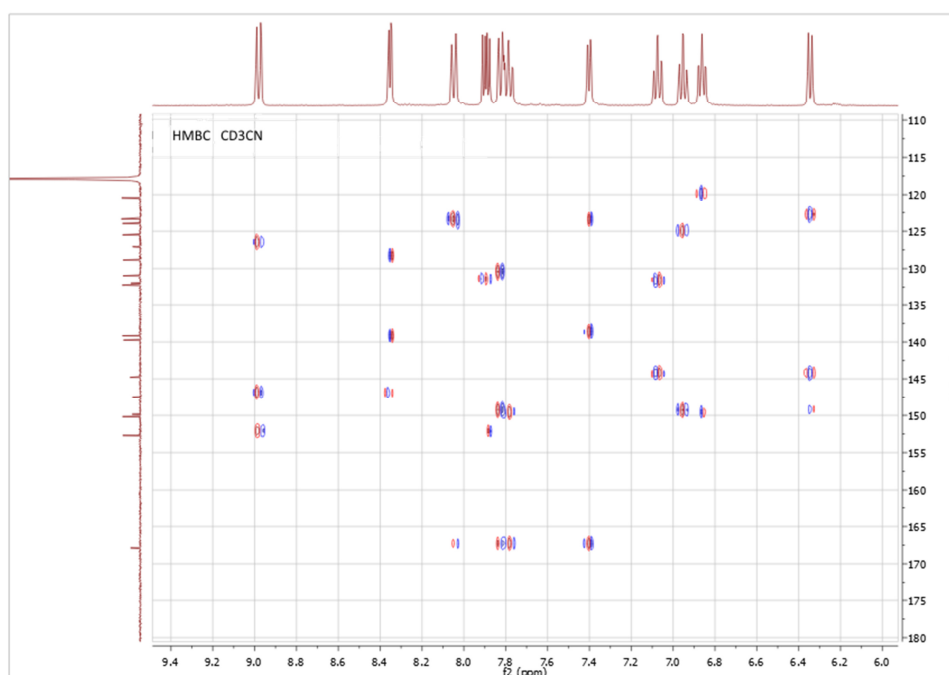


Figure S4. $^1\text{H}^{13}\text{C}$ HMBC NMR spectrum of **2**-PF₆ in CD₃CN at 300 K.

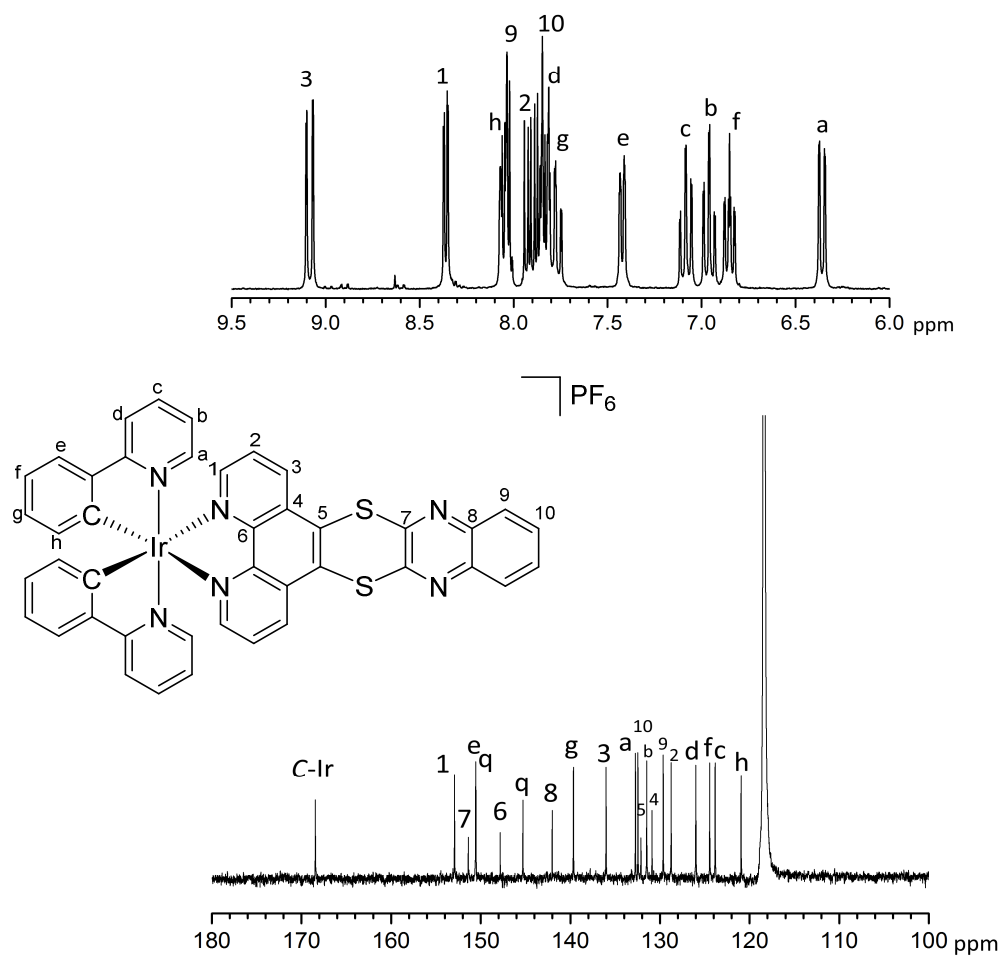


Figure S5. Top: ^1H NMR spectrum of **3**-PF₆ in CD₃CN at 300 K; bottom: ^{13}C NMR spectrum of **3**-PF₆ in CD₃CN at 300 K.

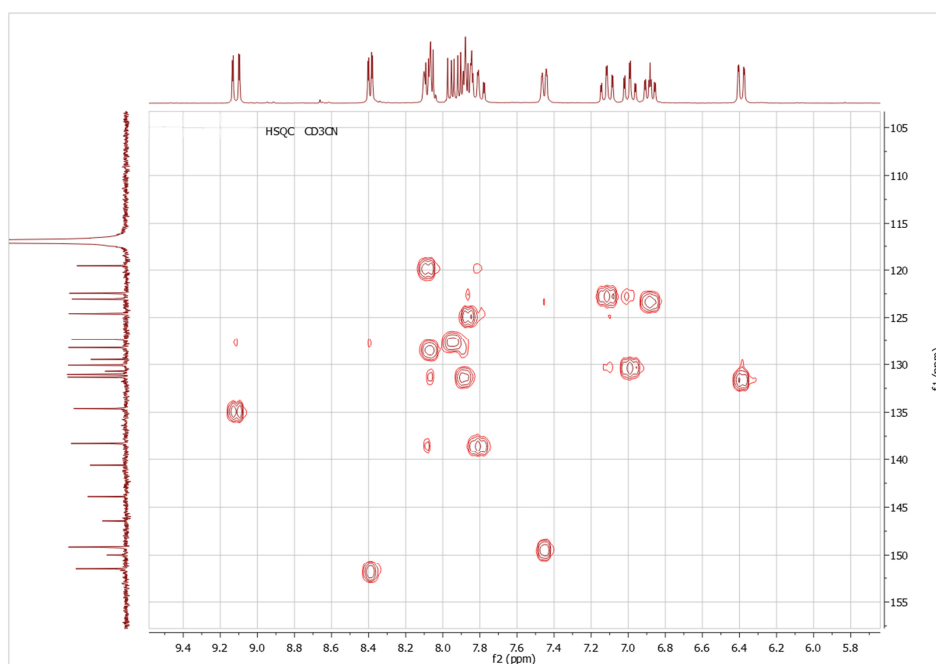


Figure S6. ^1H COSY NMR spectrum of **3**-PF₆ in CD₃CN at 300 K.

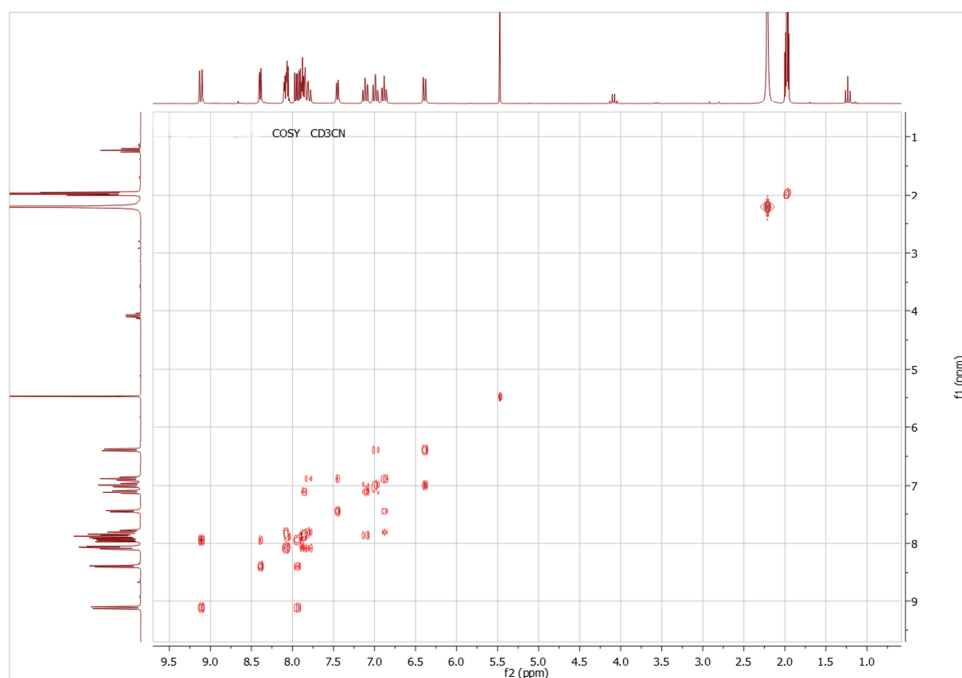


Figure S7. $^1\text{H}^{13}\text{C}$ HSQC NMR spectrum of **3**-PF₆ in CD₃CN at 300 K.

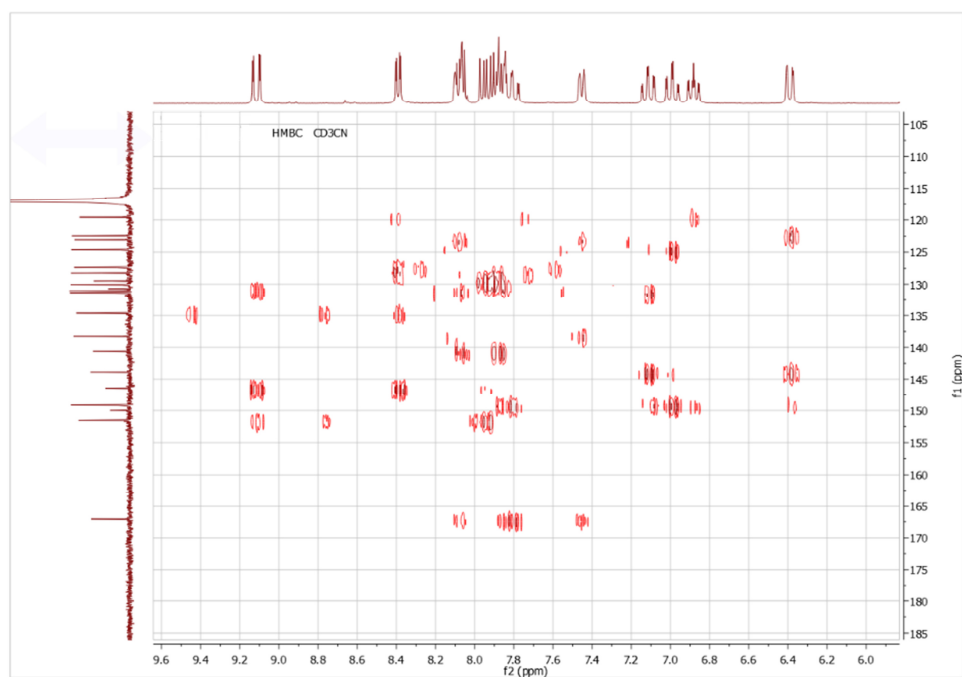


Figure S8. $^1\text{H}^{13}\text{C}$ HMBC NMR spectrum of **3**-PF₆ in CD₃CN at 300 K.

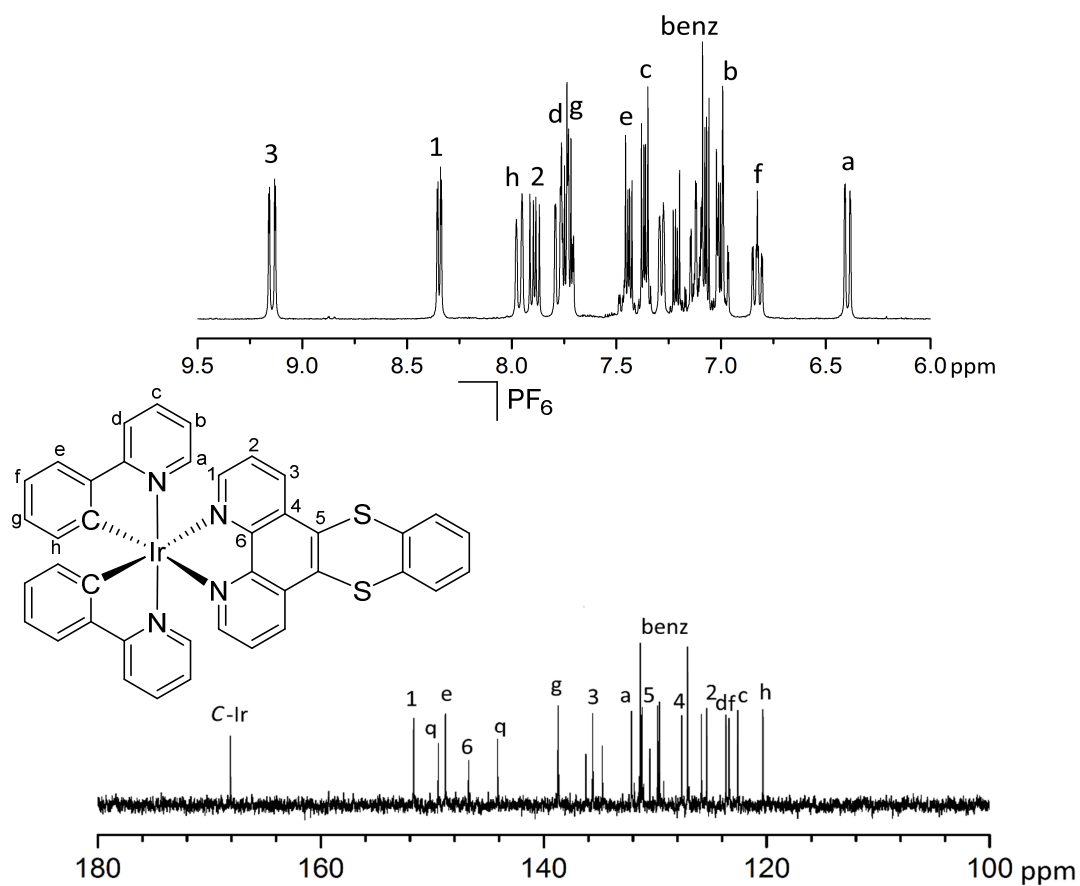


Figure S9. Top: ^1H NMR spectrum of 4-PF_6 in CD_2Cl_2 at 300 K; bottom: ^{13}C NMR spectrum of 4-PF_6 in CD_2Cl_2 at 300 K.

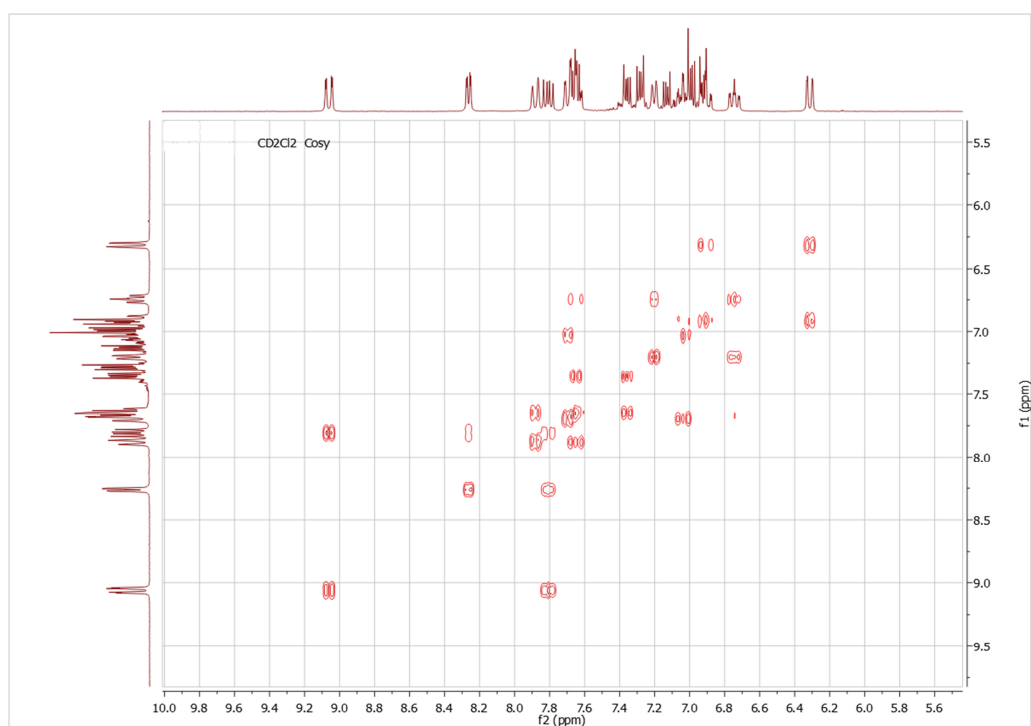


Figure S10. ^1H - ^1H COSY NMR spectrum of 4-PF_6 in CD_2Cl_2 at 300 K.

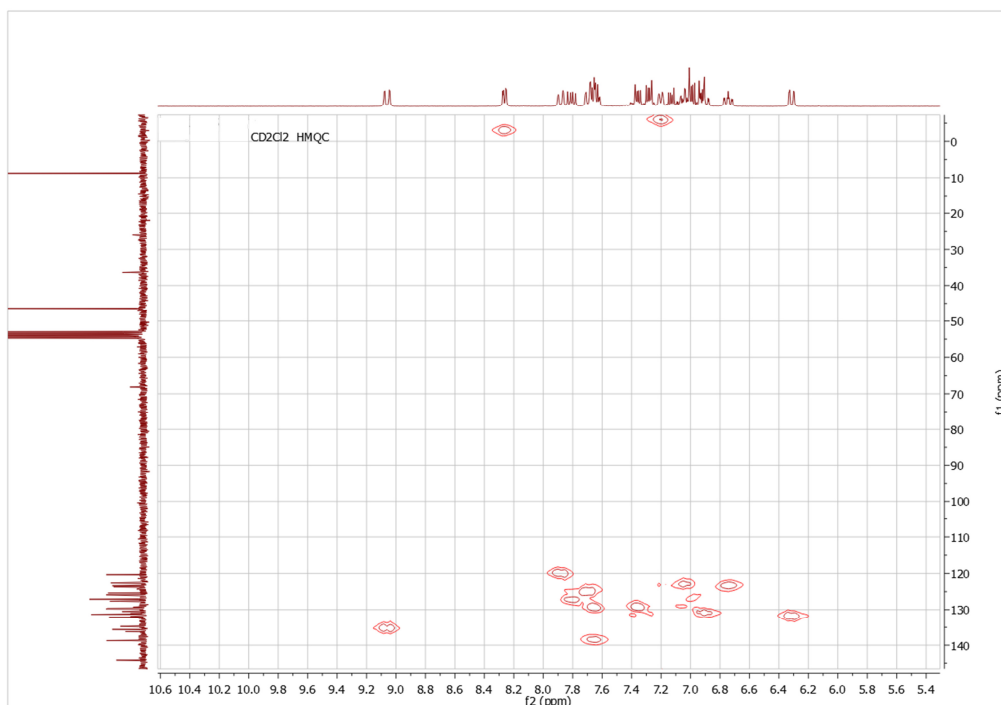


Figure S11. $^1\text{H}^{13}\text{C}$ HSQC NMR spectrum of 4-PF₆ in CD₂Cl₂ at 300 K.

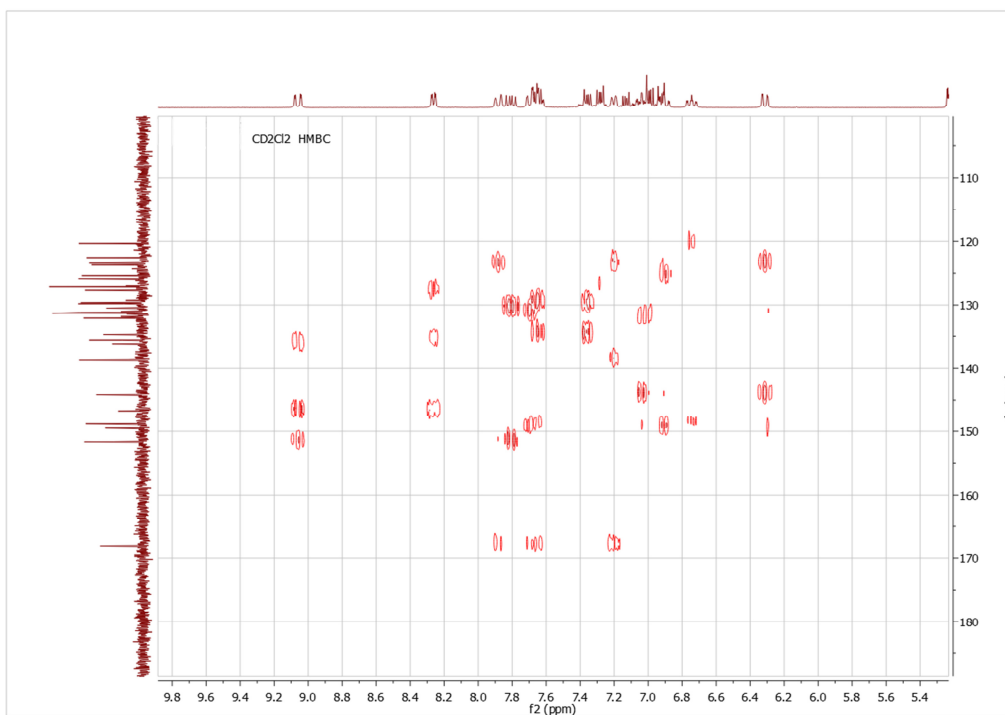


Figure S12. $^1\text{H}^{13}\text{C}$ HMBC NMR spectrum of 4-PF₆ in CD₂Cl₂ at 300 K.

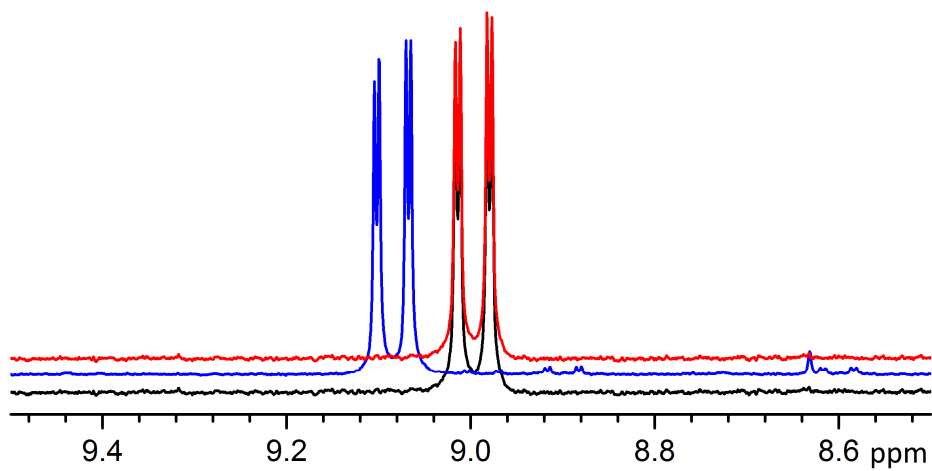


Figure S13. Comparison of ¹H NMR shift of **2-PF₆** (black), **3-PF₆** (blue) and **4-PF₆** (red) in CD₃CN at 300 K.

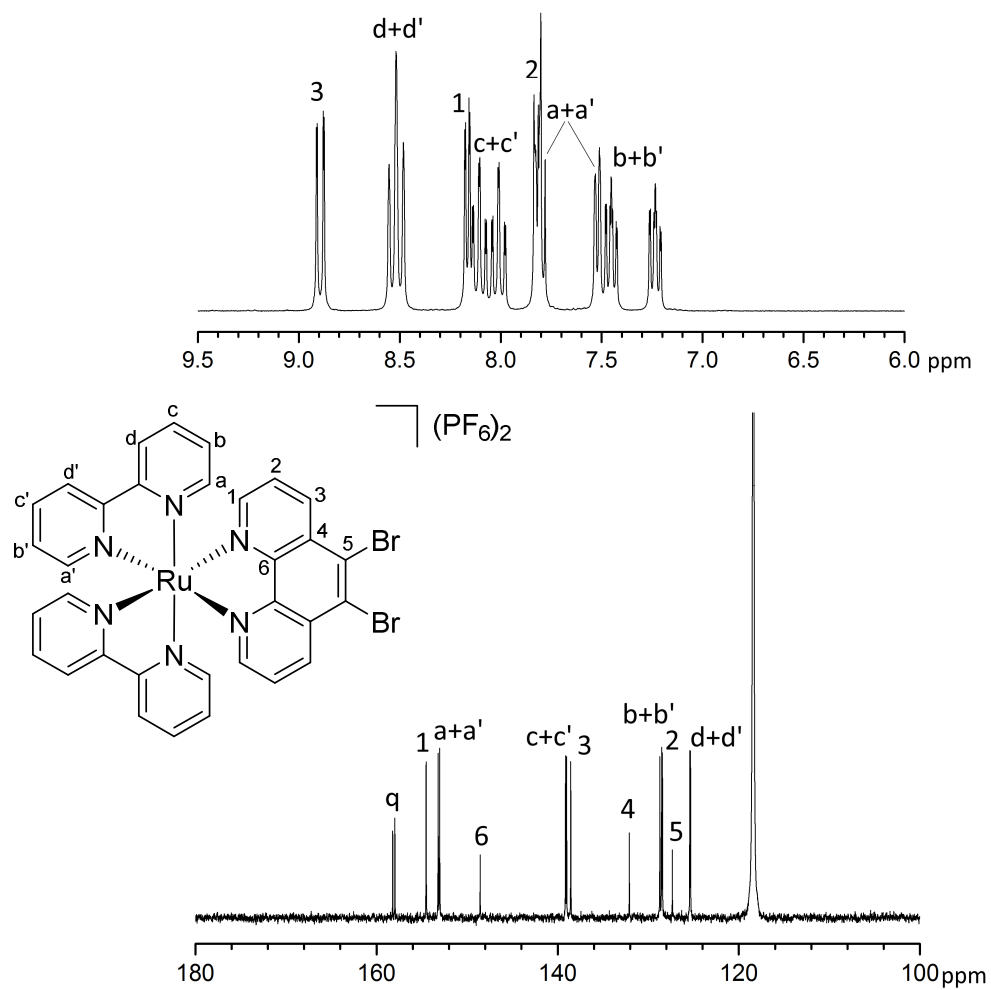


Figure S14. Top: ¹H NMR spectrum of **5-(PF₆)₂** in CD₃CN at 300 K; bottom: ¹³C NMR spectrum of **5-(PF₆)₂** in CD₃CN at 300 K.

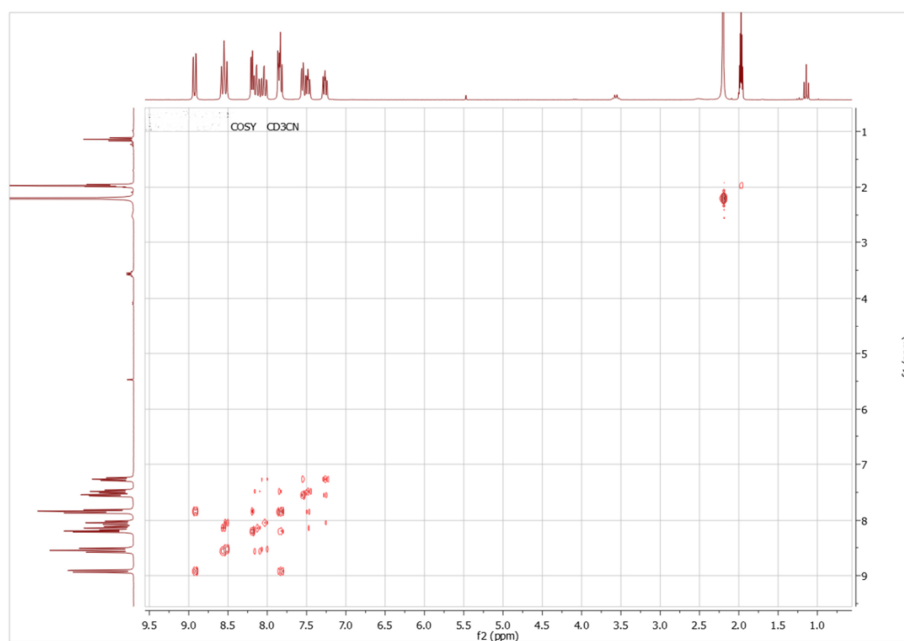


Figure S15. ¹H-¹H COSY NMR spectrum of **5-(PF₆)₂** in CD₃CN at 300 K.

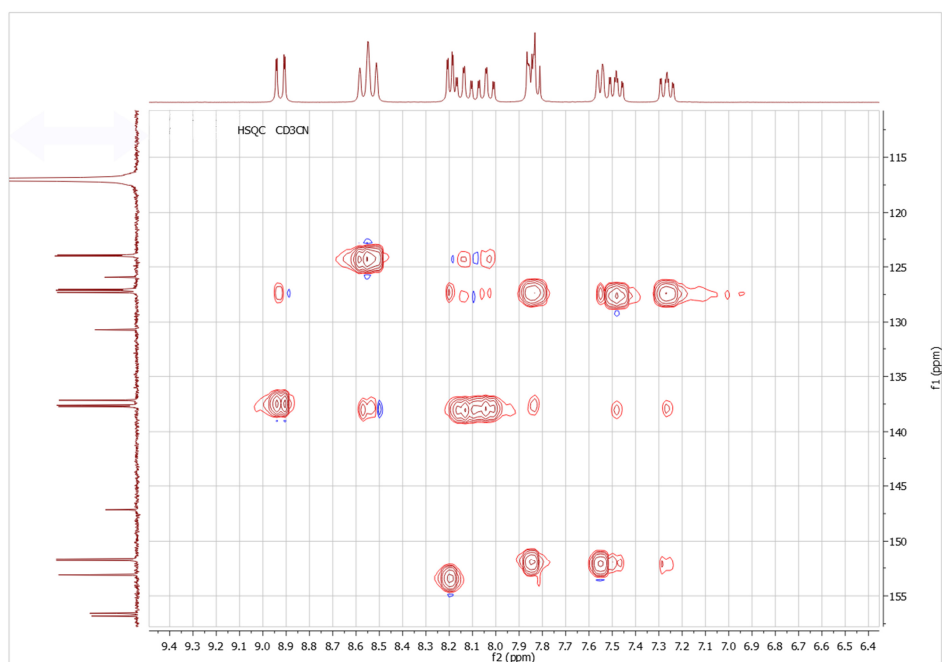


Figure S16. $^1\text{H}^{13}\text{C}$ HSQC NMR spectrum of **5**-(PF₆)₂ in CD₃CN at 300 K.

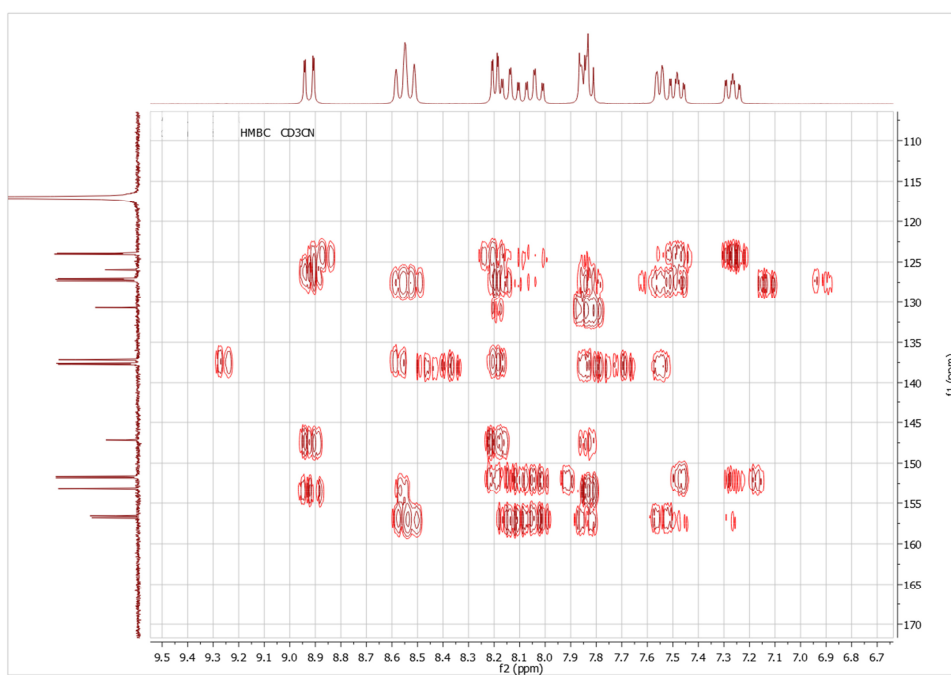


Figure S17. $^1\text{H}^{13}\text{C}$ HMBC NMR spectrum of **5**-(PF₆)₂ in CD₃CN at 300 K.

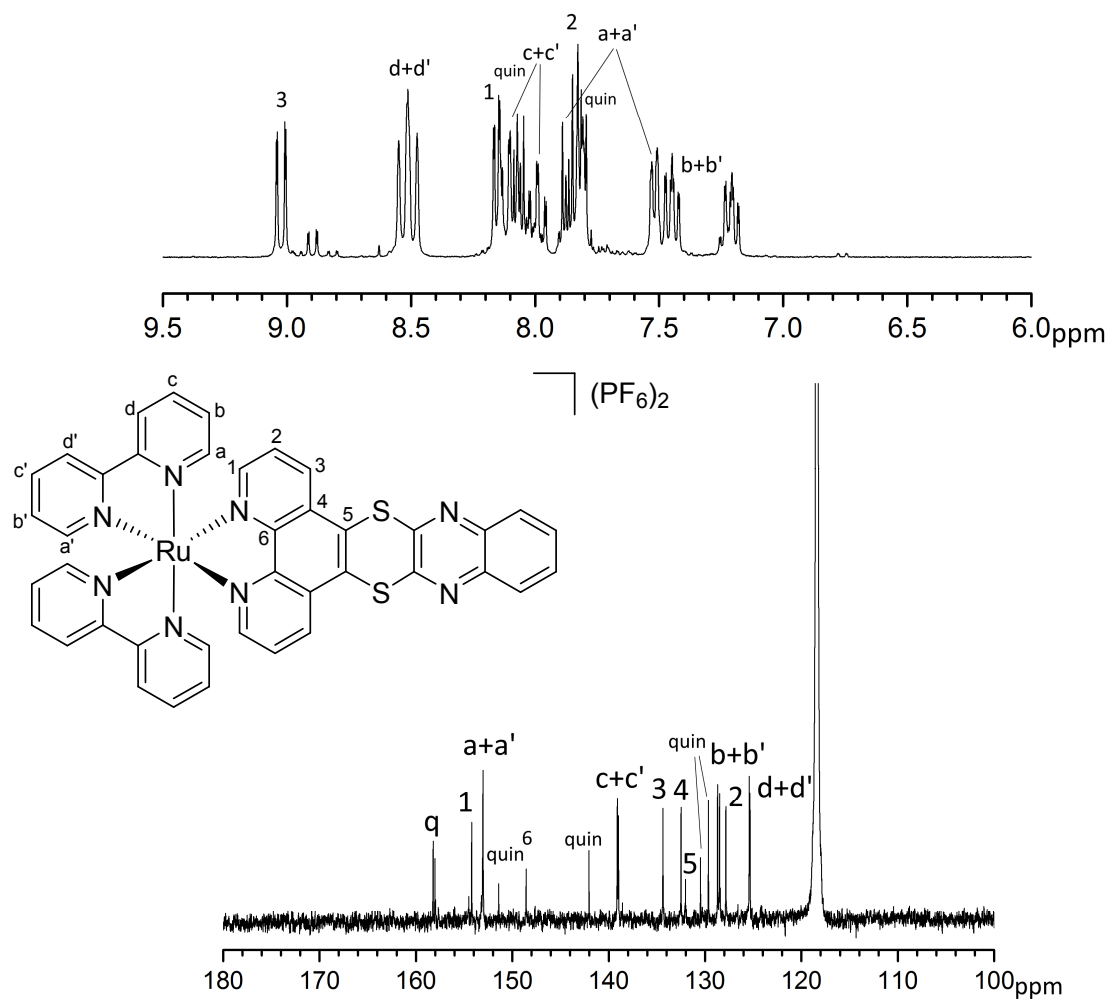


Figure S18. Top: ^1H NMR spectrum of $\mathbf{6}-(\text{PF}_6)_2$ in CD_3CN at 300 K; bottom: ^{13}C NMR spectrum of $\mathbf{6}-(\text{PF}_6)_2$ in CD_3CN at 300 K.

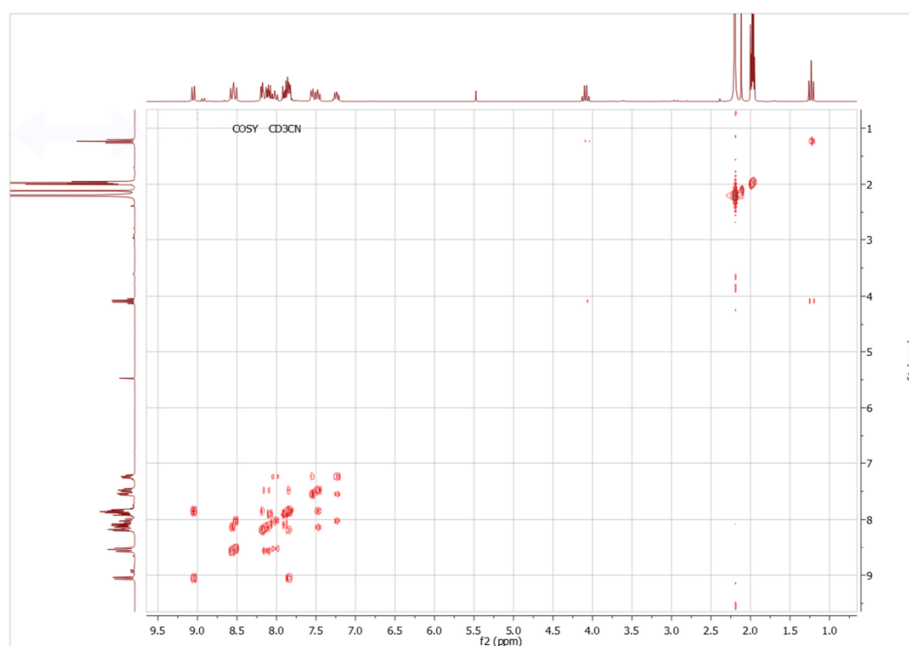


Figure S19. ^1H - ^1H COSY NMR spectrum of $\mathbf{6}-(\text{PF}_6)_2$ in CD_3CN at 300 K.

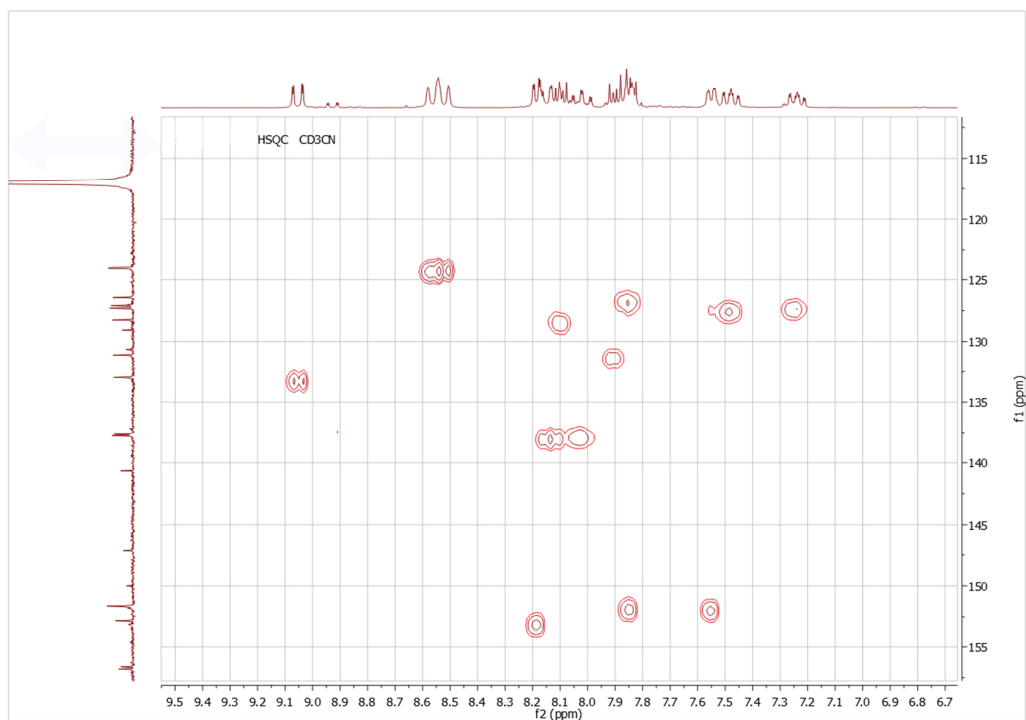


Figure S20. $^1\text{H}^{13}\text{C}$ HSQC NMR spectrum of **6**-(PF₆)₂ in CD₃CN at 300 K.

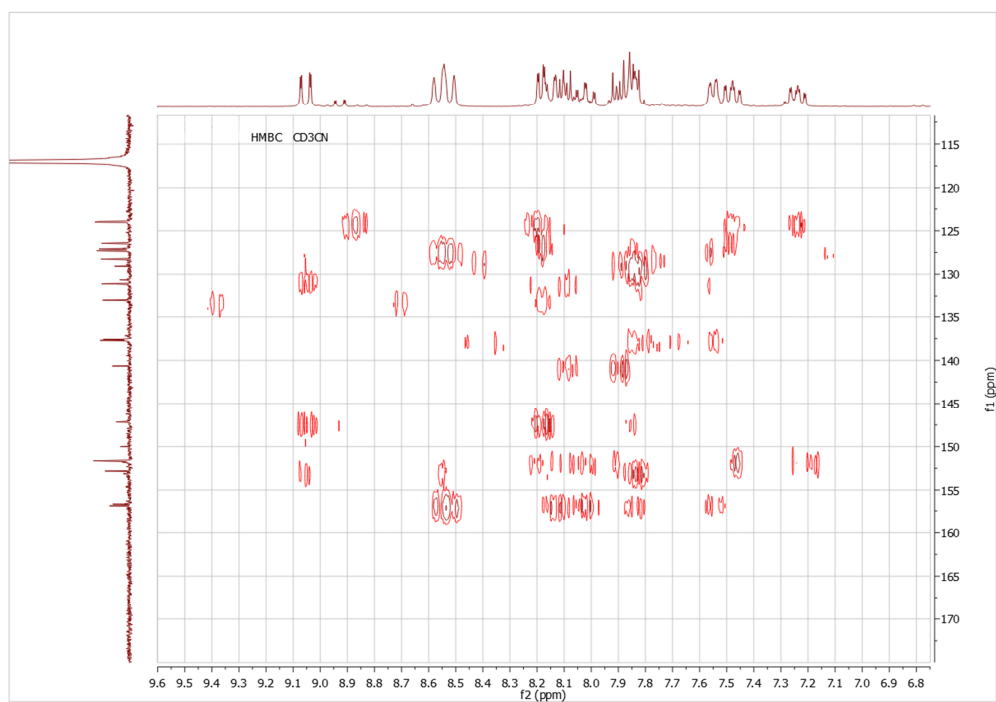


Figure S21. $^1\text{H}^{13}\text{C}$ HMBC NMR spectrum of **6**-(PF₆)₂ in CD₃CN at 300 K.

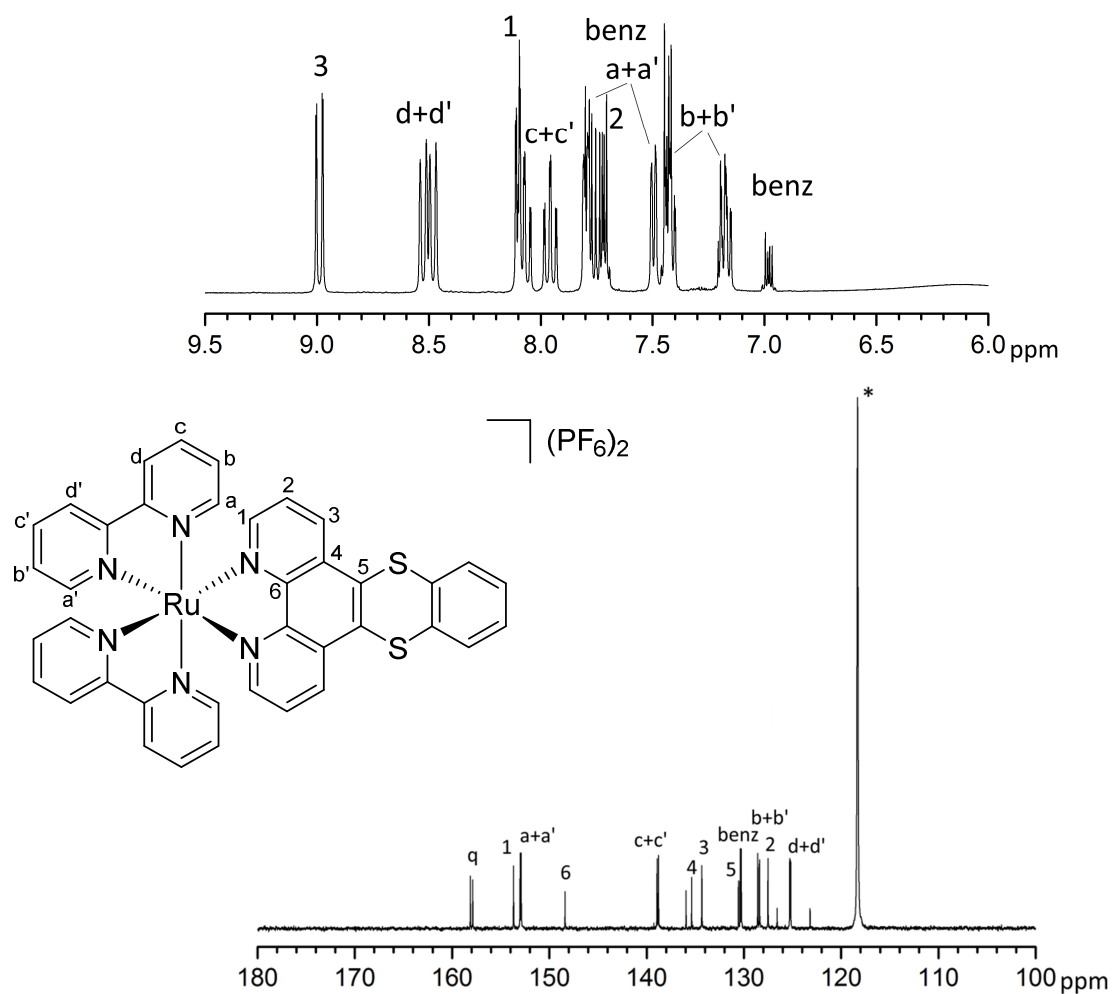


Figure S22. Top: ^1H NMR spectrum of $7\text{-(PF}_6)_2$ in CD_3CN at 300 K; bottom: ^{13}C NMR spectrum of $7\text{-(PF}_6)_2$ in CD_3CN at 300 K.



Figure S23. ^1H - ^1H COSY NMR spectrum of $7\text{-(PF}_6)_2$ in CD_3CN at 300 K.

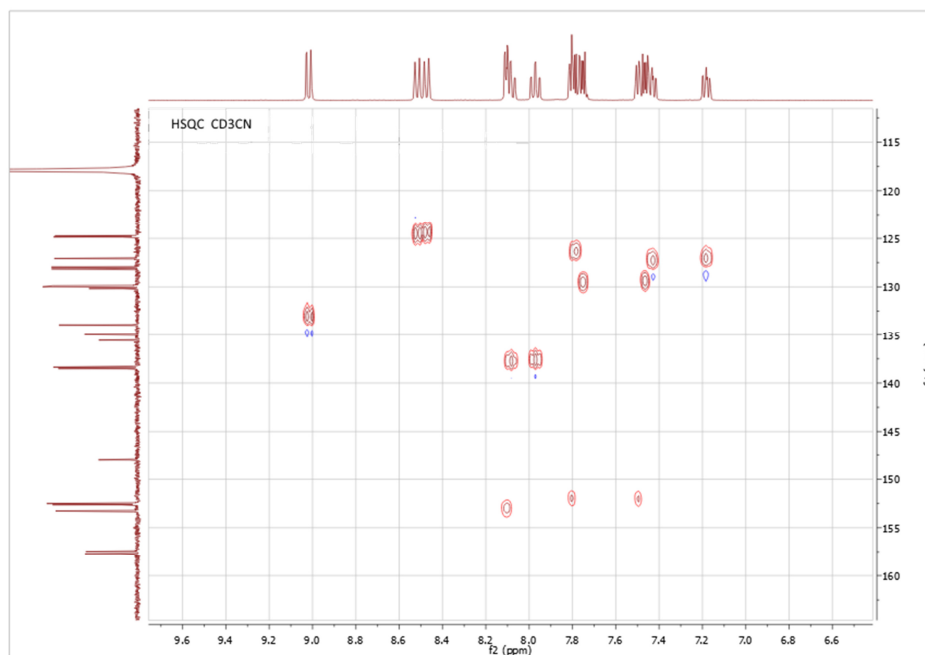


Figure S24. $^1\text{H}^{13}\text{C}$ HSQC NMR spectrum of 7-(PF₆)₂ in CD₃CN at 300 K.

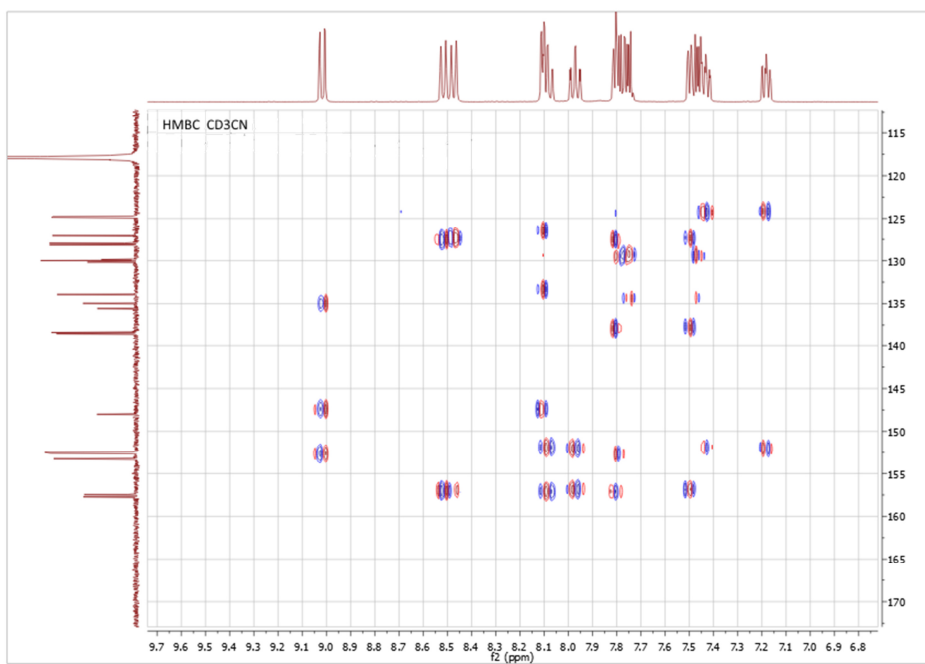


Figure S25. $^1\text{H}^{13}\text{C}$ HMBC NMR spectrum of 7-(PF₆)₂ in CD₃CN at 300 K.

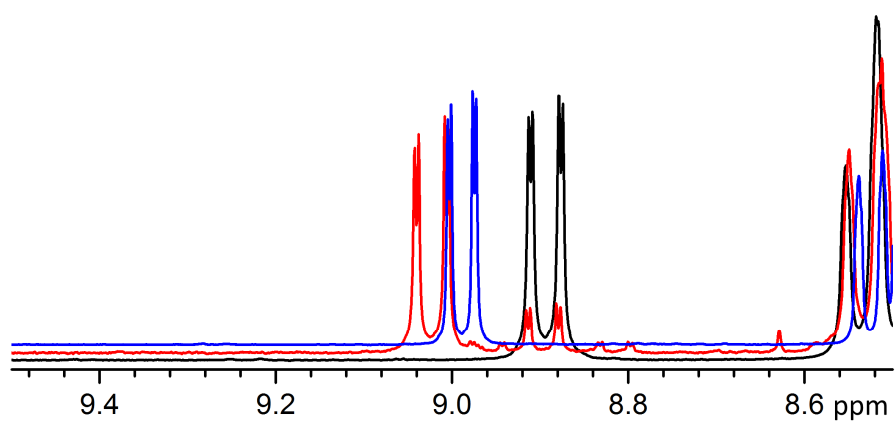


Figure S26. Comparison of ^1H NMR shift of **5**-(PF₆)₂ (black), **6**-(PF₆)₂ (blue) and **7**-(PF₆)₂ (red) in CD₃CN at 300 K.

II Additional information on structure, photoluminescence and absorption measurements

Structure of 2-PF₆

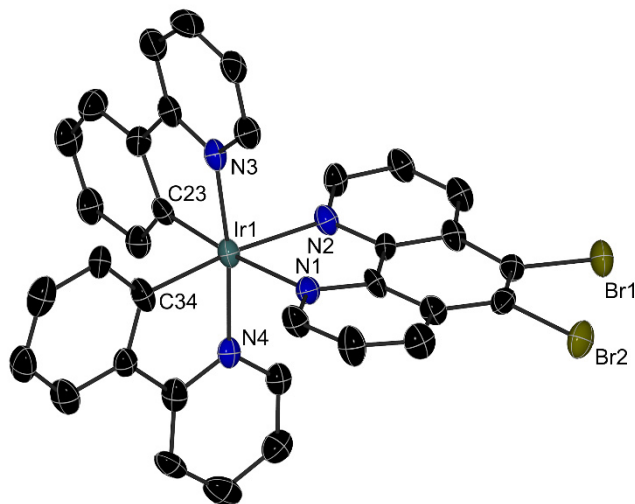


Figure S27. ORTEP representation of $[\text{Ir}(5,6\text{-dibromo-}1,10\text{-phenanthroline})(\text{ppy})_2]^+$ (2^+) with thermal ellipsoids set at 50% probability. Hydrogen atoms and counter ions were omitted for clarity.

Table S1. Crystallographic Details of Compounds 2-PF₆ and 3-PF₆.

compound	2-PF ₆	3-PF ₆
empirical formula	C ₃₄ H ₂₂ Br ₂ IrN ₄ F ₆ P·CH ₂ Cl ₂ ·CH ₃ CN	C ₄₂ H ₂₆ IrN ₆ S ₂ F ₆ P·0.5(CH ₂ Cl ₂)
FW (g mol ⁻¹)	1109.53	1058.44
cryst syst	monoclinic	monoclinic
space group	P2 ₁ /n	P2 ₁
a (Å)	14.2184(19)	22.4564(8)
b (Å)	13.7802(9)	13.5405(5)
c (Å)	19.1871(12)	25.1871(9)
α (deg)	90.00	90.00
β (deg)	97.389(2)	91.785(2)
γ (deg)	90.00	90.00
V (Å ³)	3728.1(4)	7654.9(2)
Z	4	8
μ (mm ⁻¹)	5.98	3.782
measured reflns	42814	117421
indep reflns	9740	399574
reflns with I > 2σ(I)	5929	26368
R _{int}	0.064	0.0593
R1 (F[I > 2σ(I)])	0.052	0.0512
wR2 (F ₂ [all data])	0.122	0.1116
GOF	0.961	1.018
params	433	2114
CCDC	1823808	1823809

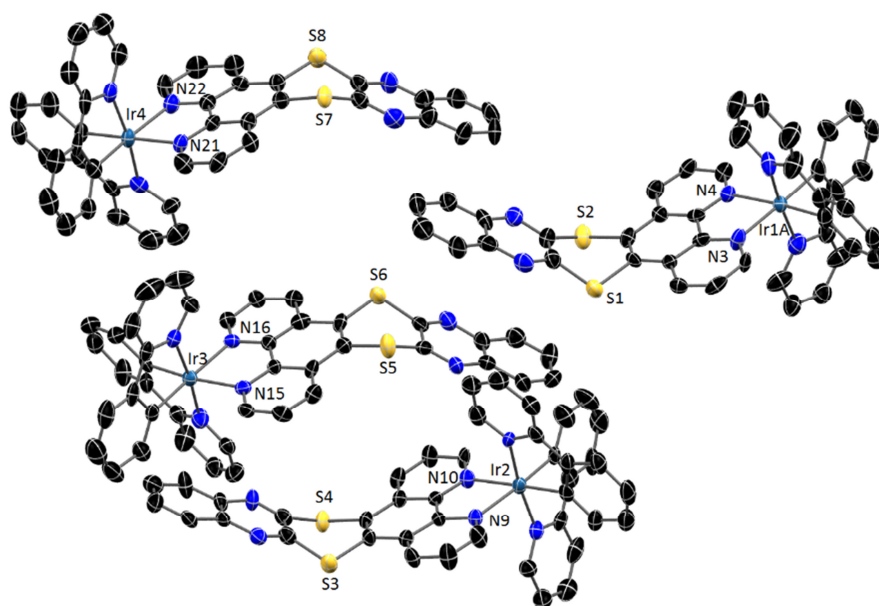


Figure S28. ORTEP representation of the elemental cell of **3**-PF₆ with thermal ellipsoids set at 50% probability. Hydrogen atoms and counter ion were omitted for clarity.

Table S2 Selected bond distances and angles from the four structured in the elemental cell of **3**-PF₆.

Bond [Å]		Angle [°]	
Ir1A-N1A	2.04(1)	N3-Ir1A-N4	78.3(4)
Ir1A-N2A	2.01(1)	C34-S2-C36	101.8(7)
Ir1A-N3	2.15(1)	C33-S1-C35	102.7(7)
Ir1A-N4	2.10(1)	C34-S2-S1-C35	133.9(8)
Ir1A-C1A	2.00(1)		
Ir1A-C12A	2.06(1)		
S2-C34	1.77(1)		
S2-C36	1.75(2)		
S1-C33	1.78(1)		
S1-C35	1.73(2)		
S1-S2	3.283(6)		
Ir2-N7	2.06(1)	N9-Ir2-N10	76.9(4)
Ir2-N8	2.02(1)	C75-S3-C77	103.7(6)
Ir2-N9	2.13(1)	C76-S4-C78	105.1(6)
Ir2-N10	2.165(9)	C76-S4-S3-C77	137.1(8)
Ir2-C43	2.03(1)		
Ir2-C54	2.02(1)		
S3-C75	1.78(1)		
S3-C77	1.77(1)		
S4-C76	1.76(1)		
S4-C78	1.78(2)		
S3-S4	3.285(5)		

Ir3-N13	2.041(9)	N15-Ir3-N16	77.2(4)
Ir3-N14	2.05(1)	C118-S5-C120	101.8(7)
Ir3-N15	2.17(1)	C117-S6-C119	103.1(6)
Ir3-N16	2.12(1)	C117-S6-S5- C120	134.9(8)
Ir3-C85	2.02(1)		
Ir3-C96	1.997(9)		
S5-C188	1.76(1)		
S5-C120	1.77(2)		
S6-C117	1.73(1)		
S6-C119	1.77(1)		
S5-S6	3.298(5)		
Ir4-N19	2.05(1)	N21-Ir4-N22	76.9(4)
Ir4-N20	2.05(1)	C159-S7-C161	101.3(7)
Ir4-N21	2.14(1)	C160-S8-C162	103.7(7)
Ir4-N22	2.15(1)	C161-S7-S8- C160	138.2(8)
Ir4-C127	2.02(2)		
Ir4-C138	2.01(1)		
S7-C159	1.79(1)		
S7-C161	1.64(2)		
S8-C160	1.76(2)		
S8-C162	1.74(1)		
S7-S8	3.273(5)		

Time dependent measurements

Figure S29 to S37 show the result of the time-resolved photoluminescence measurements of **2-PF₆** to **4-PF₆** and **5-(PF₆)₂** to **7-(PF₆)₂** in acetonitrile. Analysis of the photoluminescence decay curves vs. time was performed with DataAnalysis provided by Horiba. The quality of fit was assessed by the χ^2 value. All measured PL decay curves could be fitted mono-exponentially. Excitation with DeltaDiod at 370 and for Ru(II) complexes also with 450 nm. For the long decay of **5-PF₆** a LED excitation at 370 nm was used.

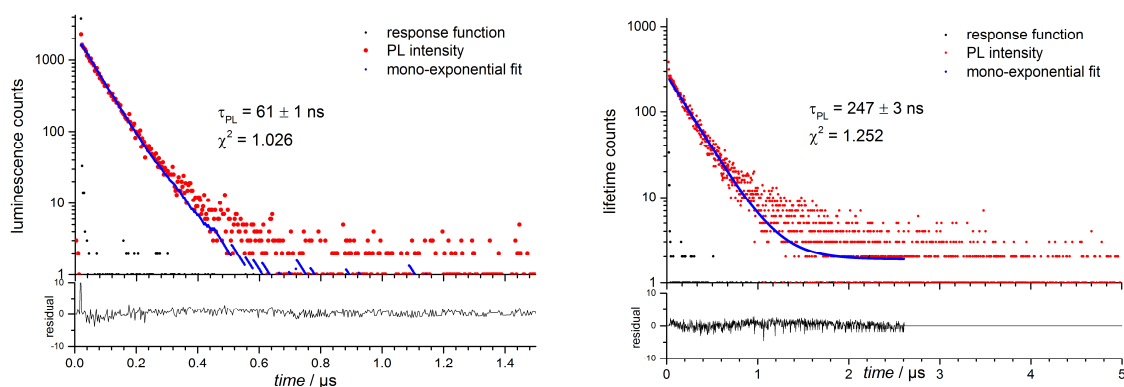


Figure S29. Emission decay curves and fits for **2-PF₆** in left: air-equilibrated and right: degassed acetonitrile ($\lambda_{exc} = 370$ nm).

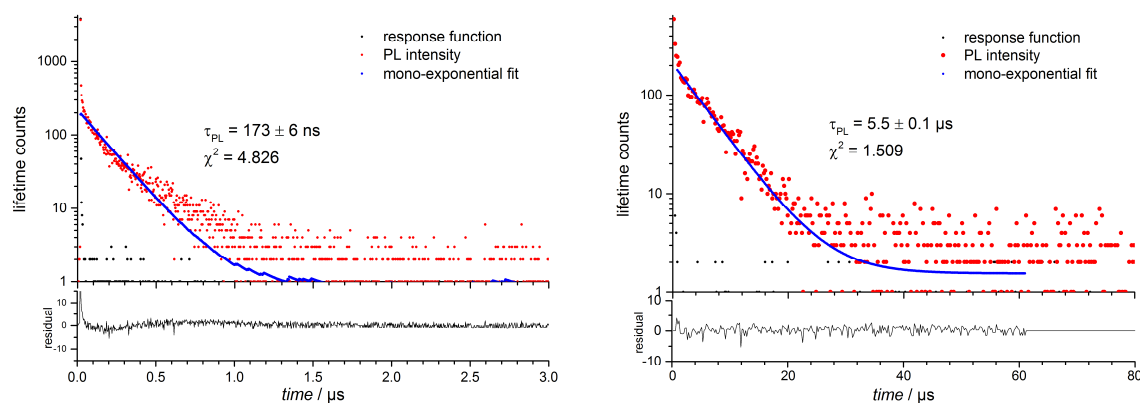


Figure S30. Emission decay curves and fits for **3-PF₆** in left: air-equilibrated and right: degassed acetonitrile ($\lambda_{exc} = 370$ nm).

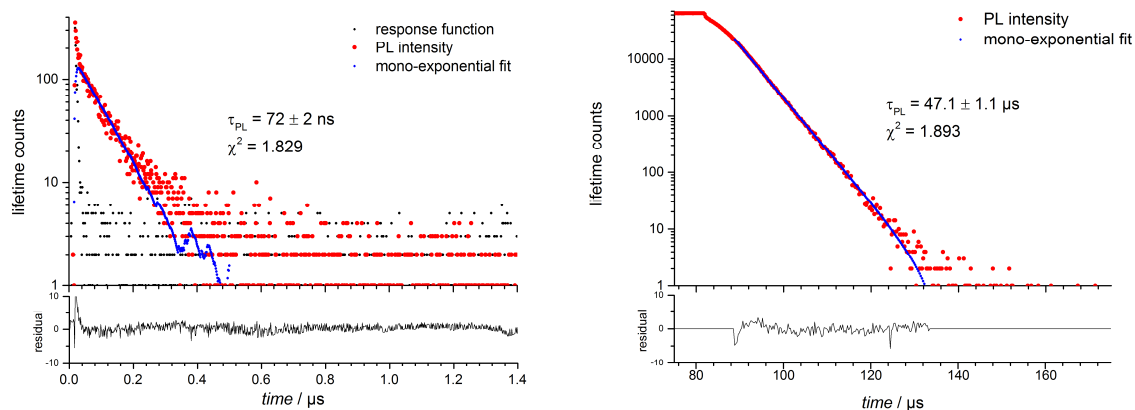


Figure S31. Emission decay curves and fits for **4-PF₆** in left: air-equilibrated and right: degassed acetonitrile ($\lambda_{\text{exc}} = 370 \text{ nm}$).

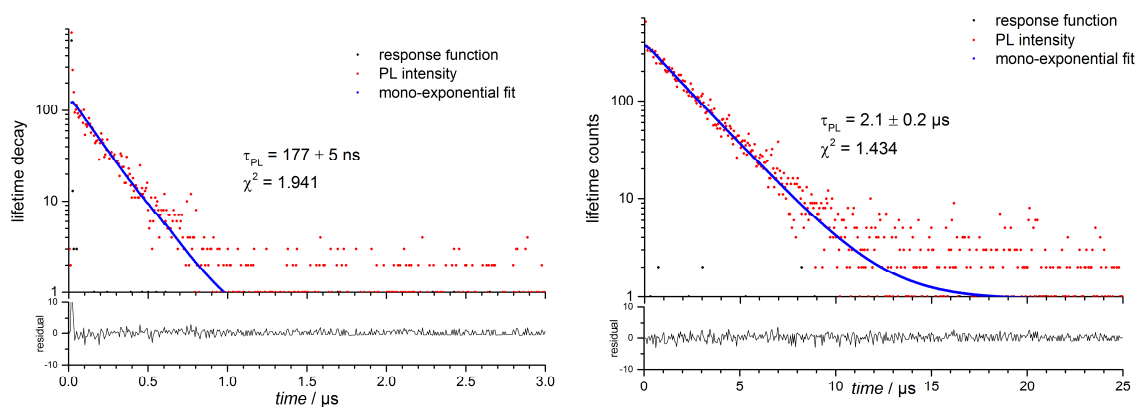


Figure S32. Emission decay curves and fits for **5-(PF₆)₂** in left: air-equilibrated and right: degassed acetonitrile ($\lambda_{\text{exc}} = 370 \text{ nm}$).

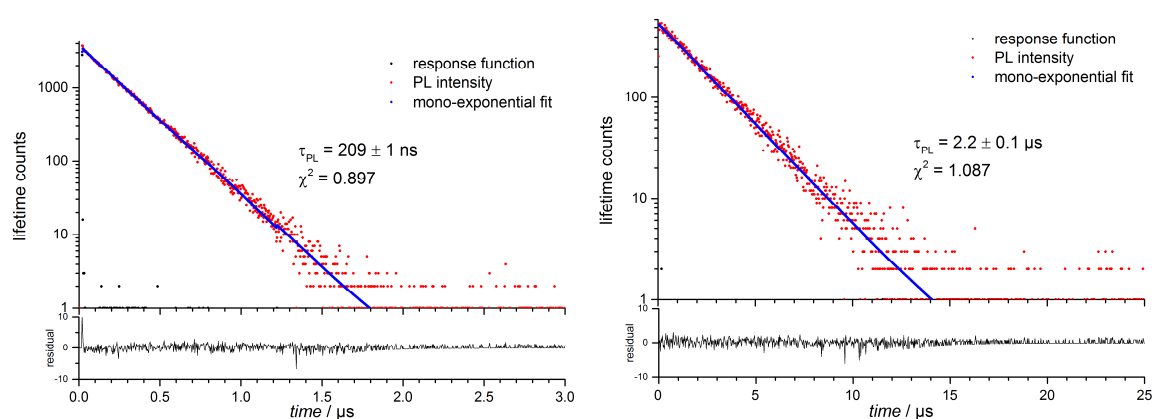


Figure S33. Emission decay curves and fits for **5-(PF₆)₂** in left: air-equilibrated and right: degassed acetonitrile ($\lambda_{\text{exc}} = 450 \text{ nm}$).

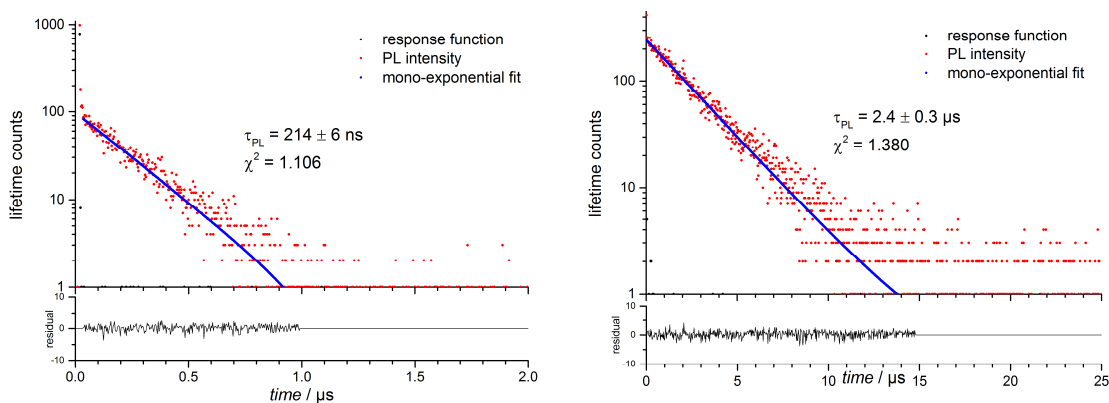


Figure S34. Emission decay curves and fits for $6-(PF_6)_2$ in left: air-equilibrated and right: degassed acetonitrile ($\lambda_{exc} = 370$ nm).

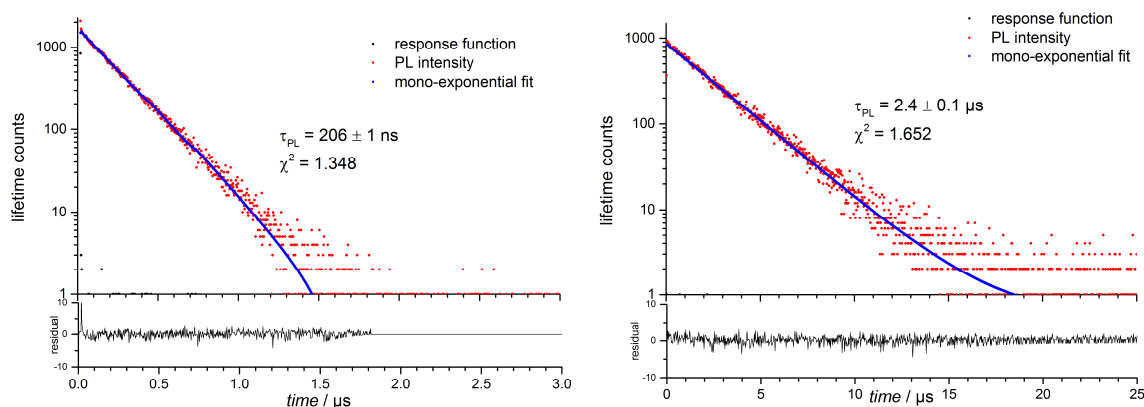


Figure S35. Emission decay curves and fits for $6-(PF_6)_2$ in left: air-equilibrated and right: degassed acetonitrile ($\lambda_{exc} = 450$ nm).

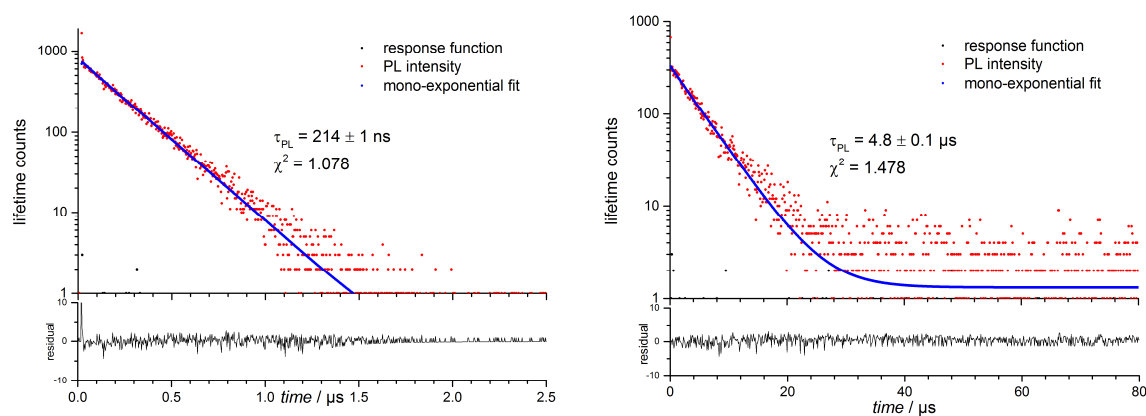


Figure S36. Emission decay curves and fits for $7-(PF_6)_2$ in left: air-equilibrated and right: degassed acetonitrile ($\lambda_{exc} = 370$ nm).

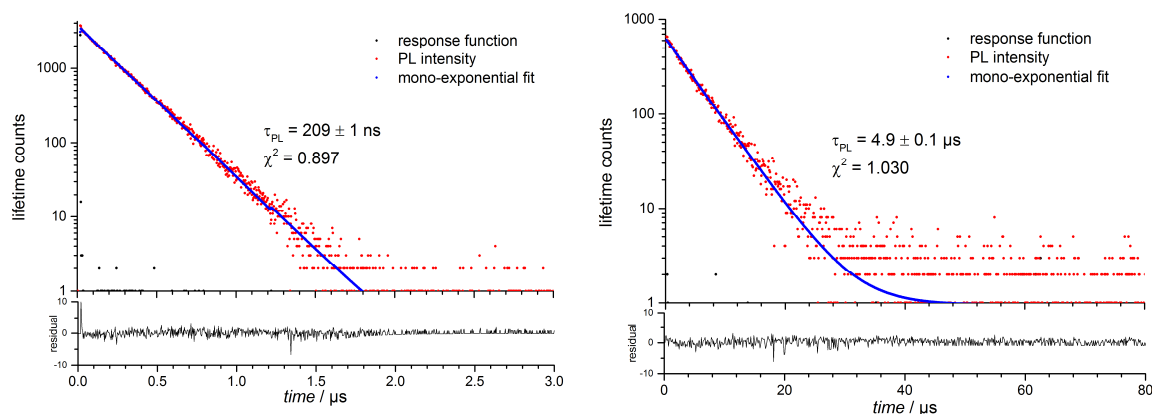


Figure S37. Emission decay curves and fits for **6-(PF₆)₂** in left: air-equilibrated and right: degassed acetonitrile ($\lambda_{\text{exc}} = 450 \text{ nm}$).

Table S3. Photophysical properties in comparison with related Ir(III) and Ru(II) phenanthroline based complexes: emission maxima at 300 K, photoluminescent quantum yields, photoluminescent lifetimes, radiative^a and nonradiative^b rate constants.

	λ_{max} (300 K) [nm]	ϕ_{PL} (degassed)	τ_{PL} (degassed) [μs]	k_{r} [s^{-1}]	k_{nr} [s^{-1}]
[Ir(ppy) ₂ (phen)]-PF ₆	579	0.119	0.78	$1.5 \cdot 10^5$	$1.1 \cdot 10^6$
[Ir(ppy) ₂ (dppz)] ^c -PF ₆	603	0.072	0.56	$1.3 \cdot 10^5$	$1.7 \cdot 10^6$
2 -PF ₆	620	0.054 ± 0.006	$0.247 \pm 0.003^{\text{a}}$	$2.2 \cdot 10^5$	$3.8 \cdot 10^6$
3 -PF ₆	615	0.056 ± 0.006	$5.5 \pm 0.1^{\text{a}}$	$1.0 \cdot 10^4$	$1.7 \cdot 10^5$
4 -PF ₆	600	0.010 ± 0.002	$47.1 \pm 1.1^{\text{a}}$	$2.1 \cdot 10^2$	$2.1 \cdot 10^4$
[Ru(bpy) ₂ (phen)]-(PF ₆) ₂	612	0.06	0.8	$7.5 \cdot 10^4$	$1.2 \cdot 10^6$
[Ru(bpy) ₂ (phendtCO)] ^a -(PF ₆) ₂	629	0.097	2.08	$4.7 \cdot 10^4$	$4.3 \cdot 10^5$
[Ru(bpy) ₂ (tppz)] ^c -(PF ₆) ₂	628	0.045	1.09	$4.1 \cdot 10^4$	$8.7 \cdot 10^5$
5 -(PF ₆) ₂	628	0.176 ± 0.018	$2.2 \pm 0.1^{\text{b}}$	$8.0 \cdot 10^4$	$3.7 \cdot 10^5$
6 -(PF ₆) ₂	622	0.182 ± 0.020	$2.4 \pm 0.1^{\text{b}}$	$7.5 \cdot 10^4$	$3.4 \cdot 10^5$
7 -(PF ₆) ₂	615	0.056 ± 0.007	$4.9 \pm 0.1^{\text{b}}$	$1.1 \cdot 10^4$	$1.9 \cdot 10^5$

^a k_{r} = radiative rate constant ($k_{\text{r}} = \phi_{\text{PL}}/\tau_{\text{PL}}$); ^b k_{nr} = nonradiative rate constant ($k_{\text{r}} + k_{\text{nr}} = 1/\tau_{\text{PL}}$); ^c dppz = dipyrrophenazine; ^d phendtCO = 1,3-dithiolo[4,5-f][1,10]phenanthroline-2-one; ^e tppz = tetrapyrrophenazine

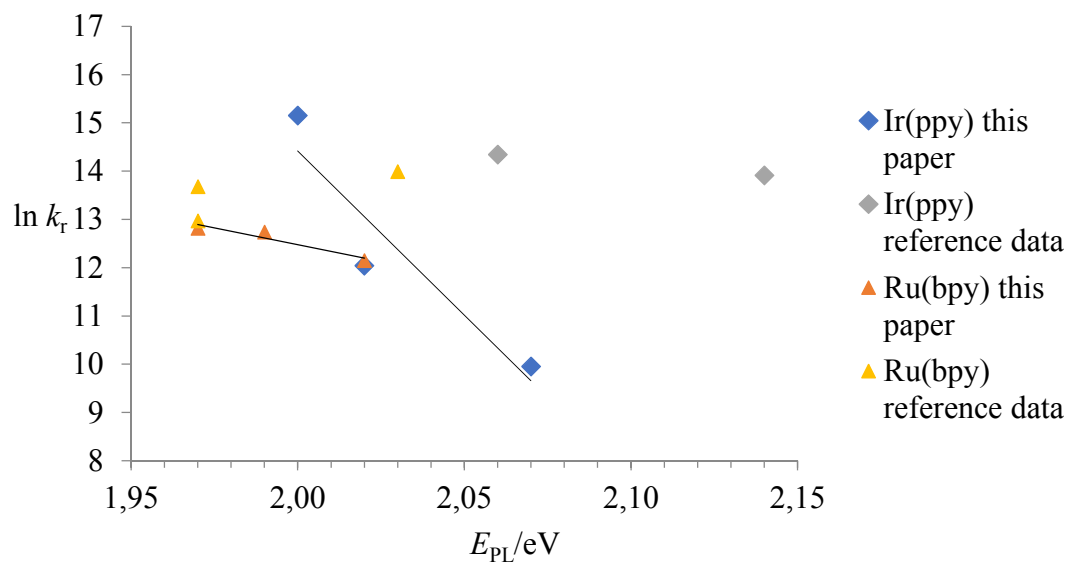


Figure S38. Relationship between the natural log of the nonradiative decay rate constant (k_{nr}) and the emission energy E_{PL} for the complexes compiled in Table 3.

Photoluminescence Spectra

Fig. S39 and S40 show the normalized excitation spectra of **2-PF₆** to **4-PF₆** and **5-(PF₆)₂** to **7-(PF₆)₂** in 2-Methyl-THF. Independently of the emission wavelength used for all complexes the same excitation spectra were received.

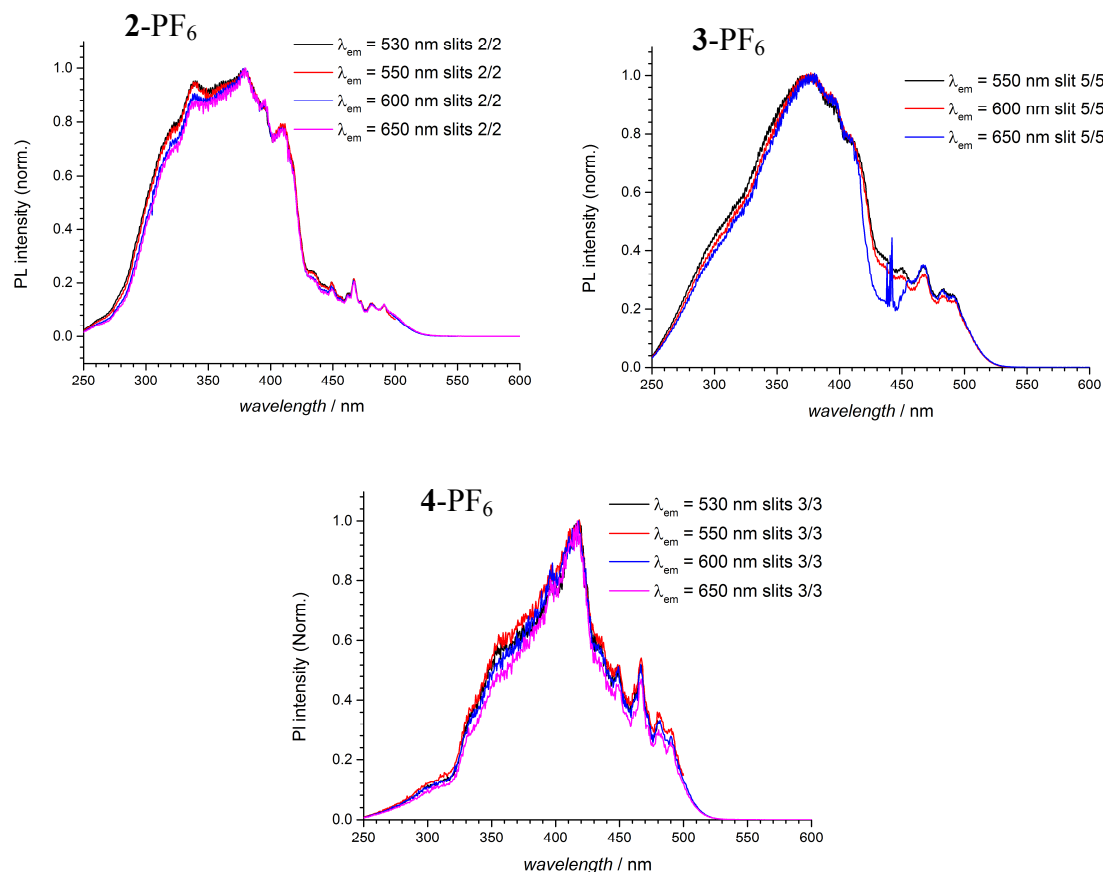


Figure S39. Uncorrected excitation spectra of **2-PF₆** to **4-PF₆** in 2-Methyl-THF. All measured excitation spectra were normalized at 1 at the individual excitation maximum. The emission wavelength as well as the employed band width of the excitation and emission slits are given in nm for the corresponding graph.

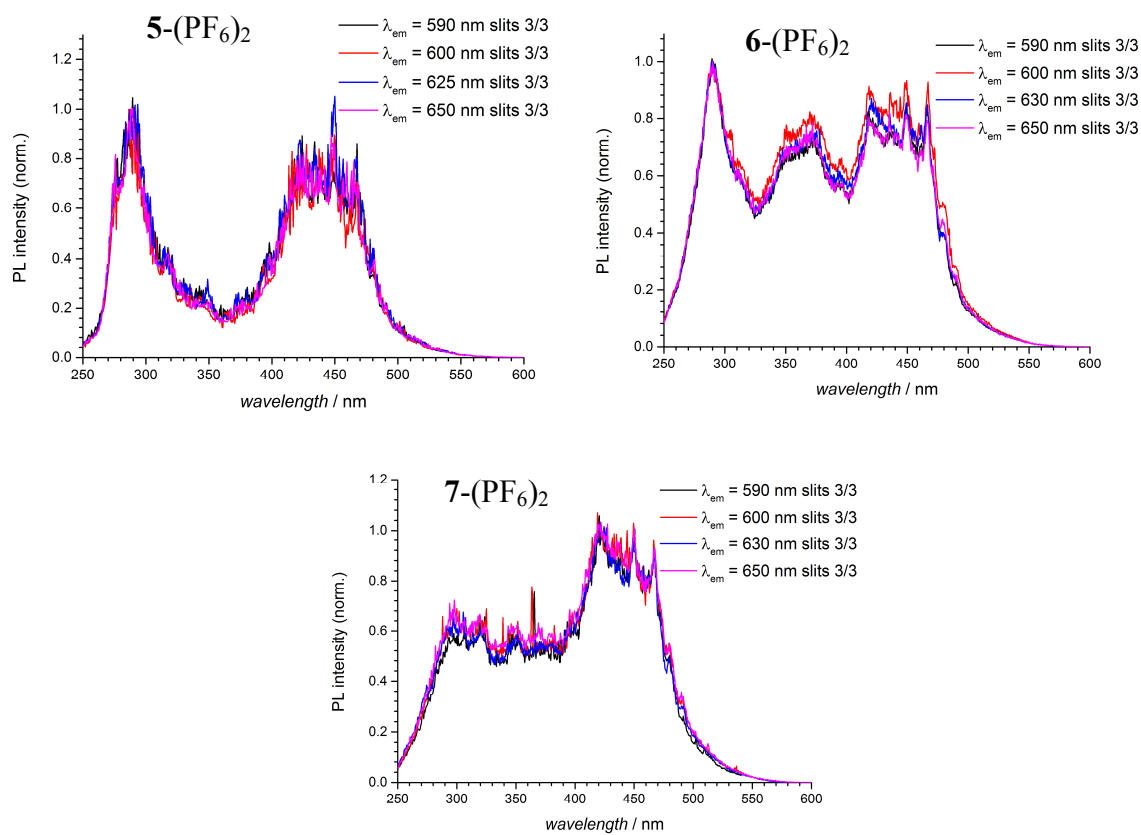


Figure S40. Uncorrected excitation spectra of **5-(PF₆)₂** to **7-(PF₆)₂** in 2-Methyl-THF. All measured excitation spectra were normalized at 1 at the individual excitation maximum. The emission wavelength as well as the employed band width of the excitation and emission slits are given in nm for the corresponding graph.

Photolumuminescence quenching with triethylamine and Stern-Volmer plots

Fig. S41 and S42 show the emission spectra of **2-PF₆** to **4-PF₆** and **5-(PF₆)₂** to **7-(PF₆)₂** in degassed acetonitrile in dependency of sequential TEA addition. The resulting Stern-Volmer plots are calculated and shown as well.

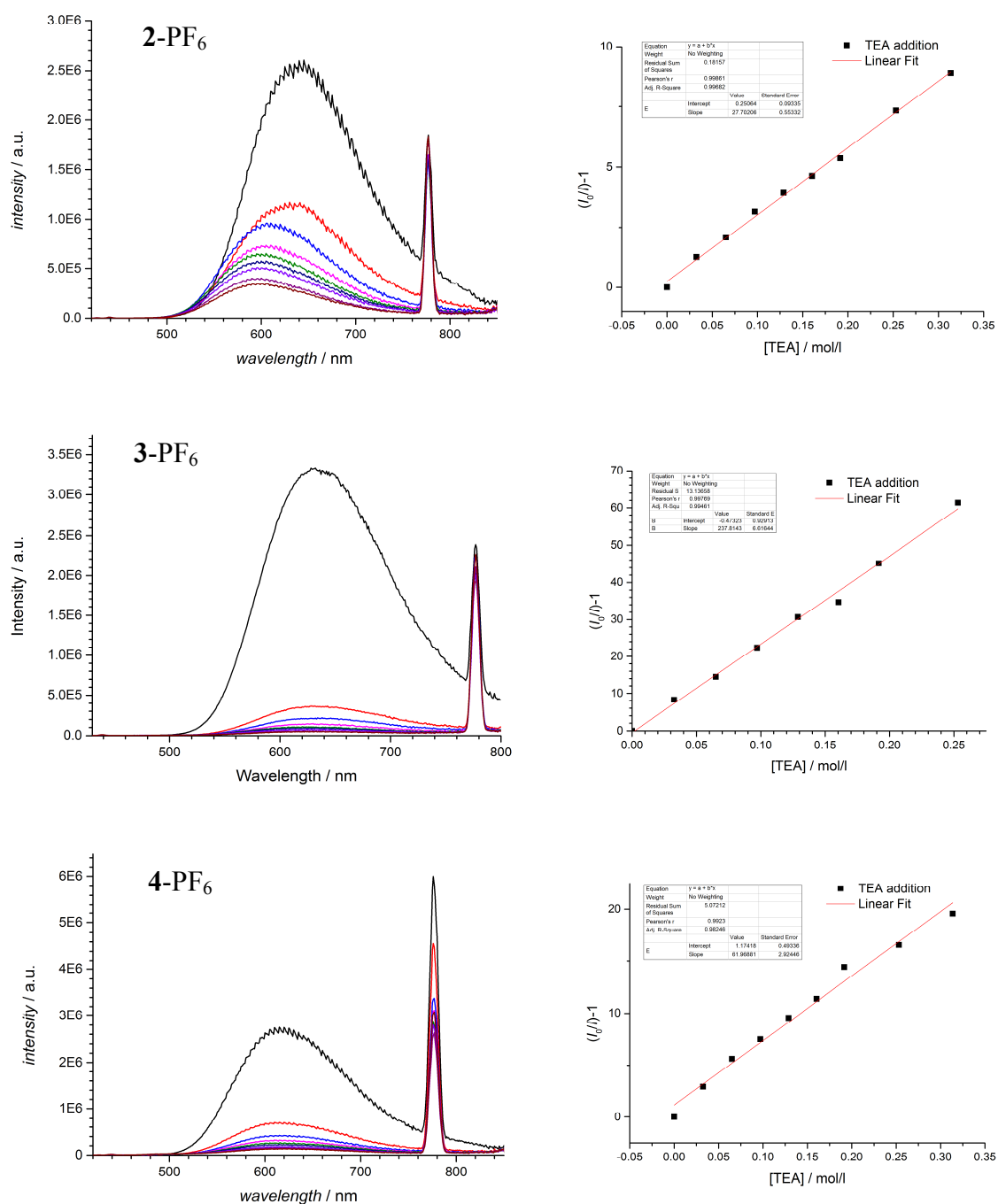


Figure S41. Left: corrected emission spectrum of **2-PF₆** to **4-PF₆** in degassed acetonitrile with sequential addition of TEA and right: corresponding Stern-Volmer plot.

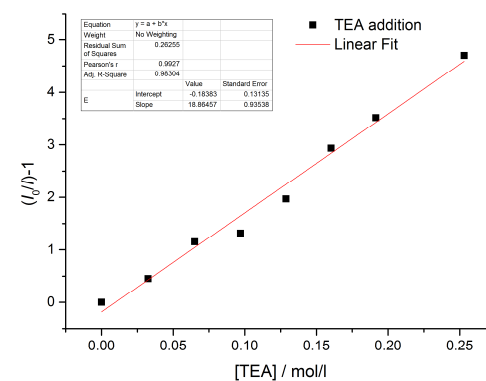
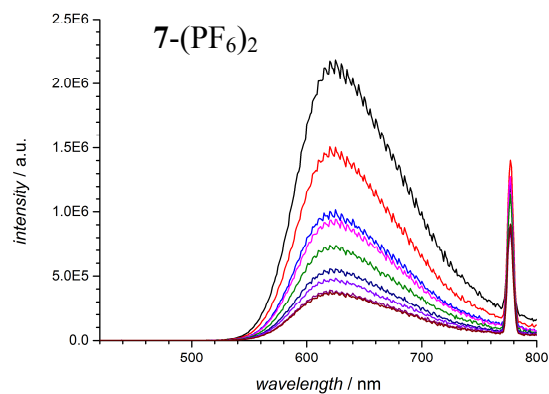
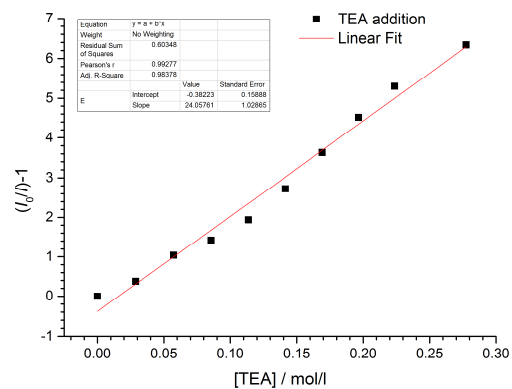
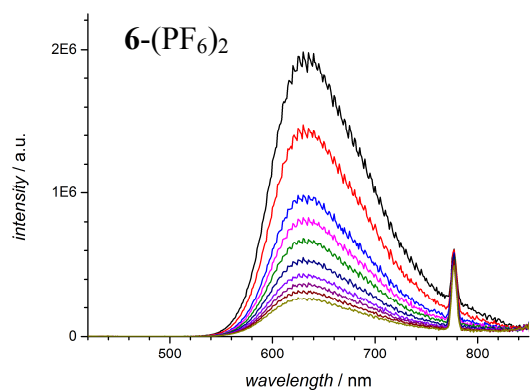
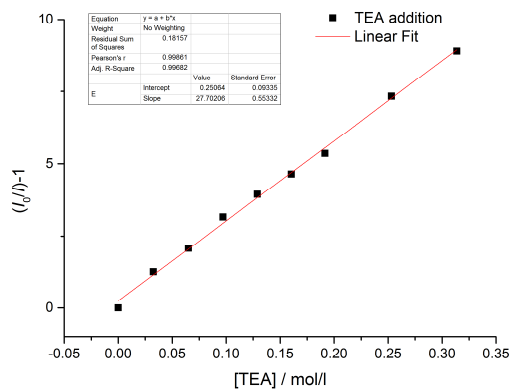
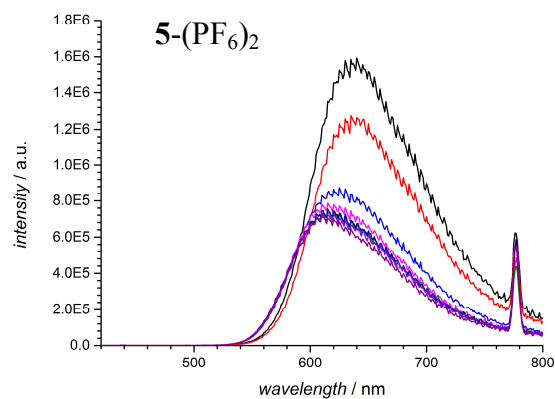


Figure S42. Left: corrected emission spectrum of **5-(PF₆)₂** to **7-(PF₆)₂** in degassed acetonitrile with sequential addition of TEA and right: corresponding Stern-Volmer plot.

III Additional information on photocatalysis

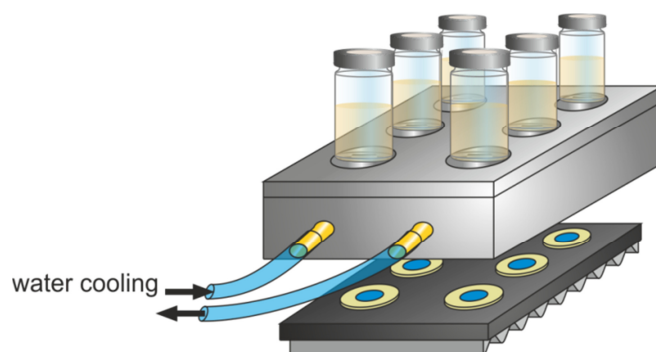


Figure S43. Irradiation setup in 5 mL crimp-top vials.

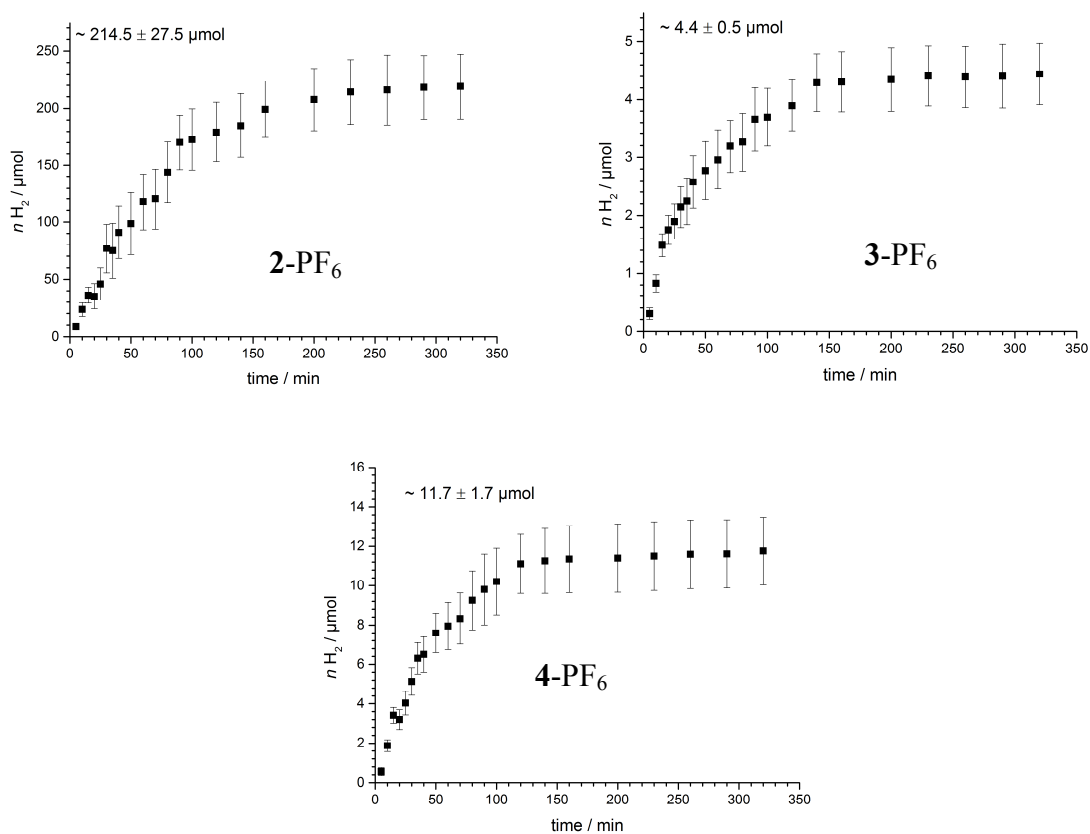


Figure S44. Dihydrogen evolution of 2-PF₆ to 4-PF₆ in solvent mixture THF:H₂O:TEA (4:3:1) with [Fe₃(CO)₁₂] as WRC.

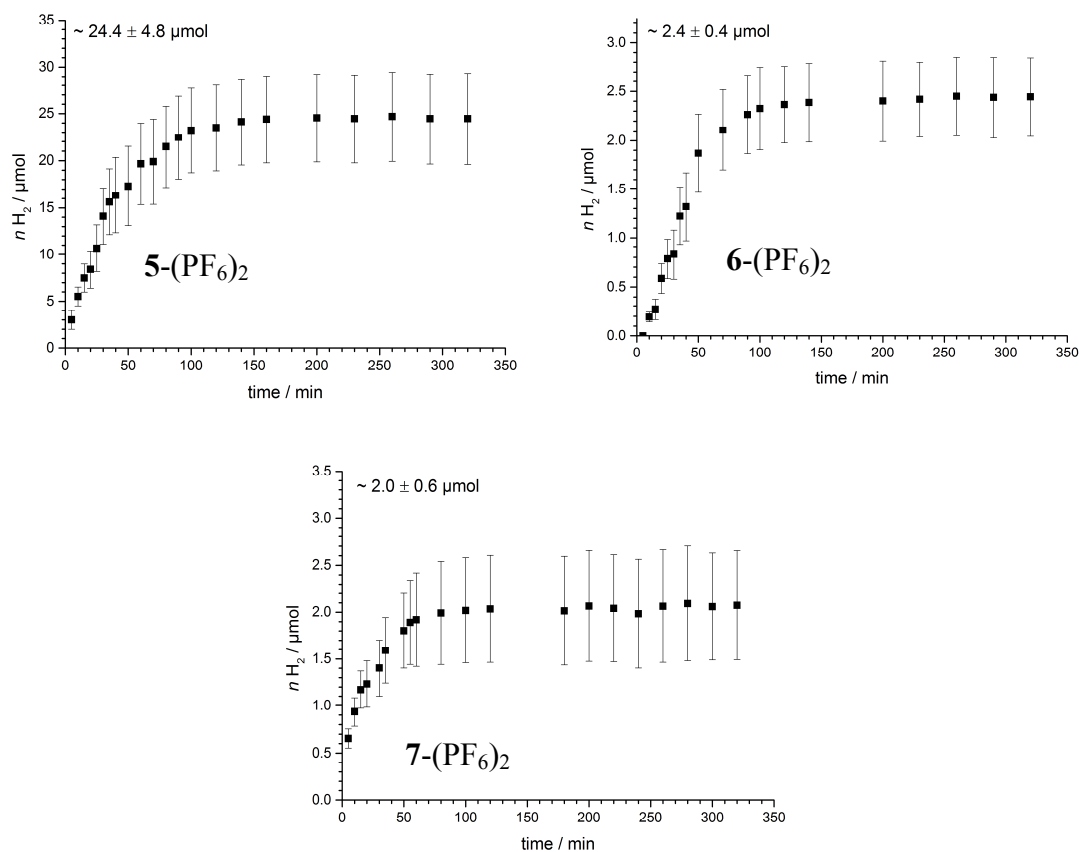


Figure S45. Dihydrogen evolution of **5-(PF₆)₂** to **7-(PF₆)₂** in solvent mixture THF:H₂O:TEA (4:3:1) with [Fe₃(CO)₁₂] as WRC.

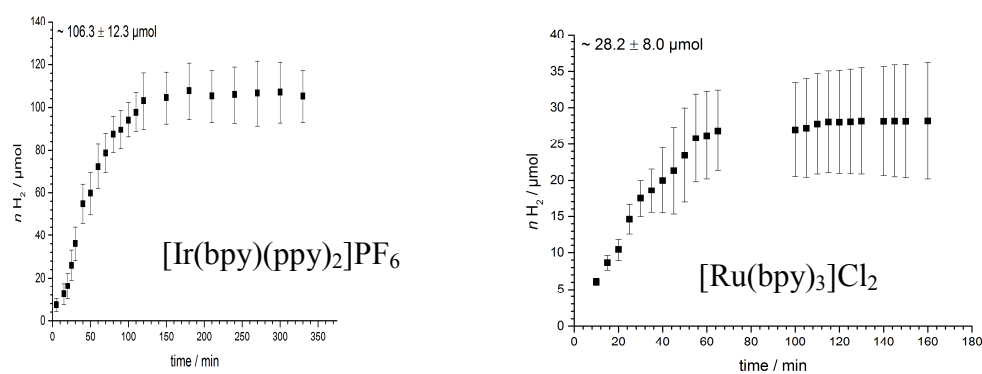


Figure S46. Dihydrogen evolution of benchmark systems in solvent mixture THF:H₂O:TEA (4:3:1) with [Fe₃(CO)₁₂] as WRC.

Online UV-vis and spectroelectrochemistry studies

To investigate the processes in the reaction mixture online UV-vis monitoring of the irradiation reaction itself and the spectroelectrochemical reduction were compared and shown exemplary for **2-PF₆** and **7-(PF₆)₂**.

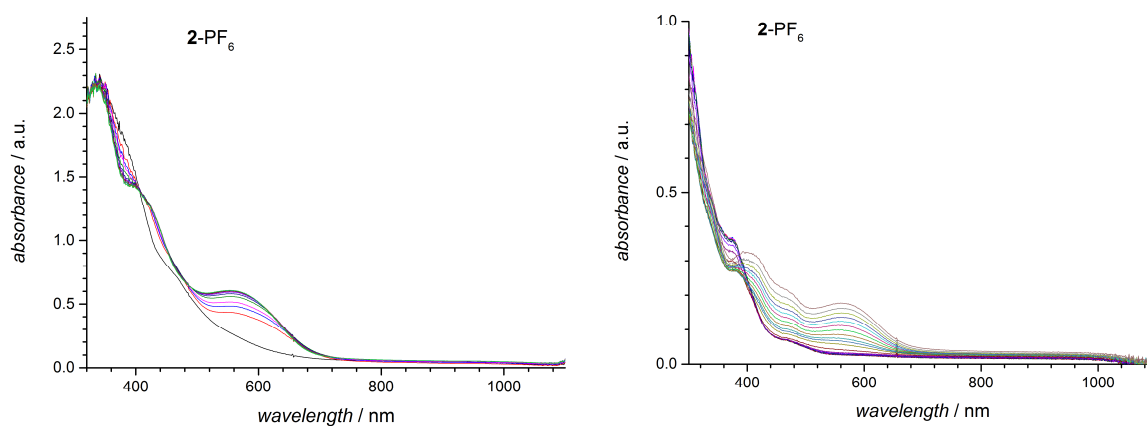


Figure S47. Left: reaction mixture of **2-PF₆** with WRC in THF:H₂O:TEA (4:3:1) during irradiation with 455 nm LED and right: electrochemical reduction of **2-PF₆** in acetonitrile using *n*Bu₄NPF₆ (0.1 M) as conducting salt.

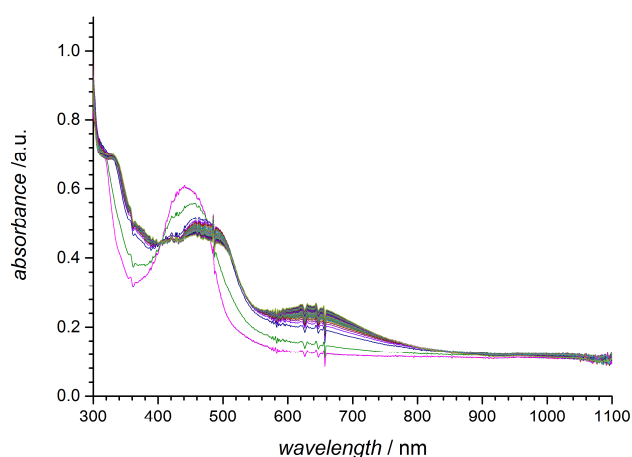


Figure S48. Solvent mixture THF:TEA:H₂O (4:3:1) and of **7-(PF₆)₂** without WRC during irradiation with 455 nm LED.